Astron. Astrophys. 349, 151–168 (1999)

ASTRONOMY AND ASTROPHYSICS

Long-term visual spectrophotometric behaviour of Be stars

II. Correlations with fundamental stellar parameters and interpretation

A. Moujtahid[1], **J. Zorec**[2], **and A.M. Hubert**[1]

[1] Observatoire de Paris-Meudon, DASGAL/UMR8633-CNRS, F-92195 Meudon Principal Cedex, France
[2] Institut d'Astrophysique de Paris, C.N.R.S. – 98^{bis}, bd. Arago, F-75014 Paris, France (zorec@iap.fr)

Received 18 May 1998 / Accepted 22 June 1999

Abstract. The long-term visual spectrophotometric (SPh) behaviour of Be stars as a function of fundamental stellar parameters is studied. Some previous SPh results obtained by other authors are confirmed. Moreover, a tendency for temperature and aspect angle dependency of SPh variations is found. From the characteristics of visual SPh behaviour in Be stars we derive constraints for models of regions in circumstellar envelopes where the visual continuum spectrum is formed: (i) The SPh emission and absorption phases should not imply preferential aspect angles, as they can both appear whatever the stellar inclination. This phenomenon cannot be always accounted for by strongly flattened circumstellar envelopes; (ii) Radii of the visible continuum forming regions cannot be larger than a few R_*; (iii) Electron densities of these regions should not exceed $N_{\rm e} \sim 10^{13}\,{\rm cm}^{-3}$; ($iv$) Electron temperature of circumstellar layers producing the SPh emission phases compare with the stellar Balmer continuum radiation temperature and it is much lower in those producing the SPh absorption phases. Three scenarios were studied to produce the observed characteristics of emissions in the V magnitude and in the second component of Balmer discontinuity (ΔD) during the SPh emission phases: (a) expansion of a massive circumstellar shell that preserves circumstellar envelope flattening; (b) expansion of a circumstellar shell which increases the global flattening, so that a disc-like structure is formed; (c) continuous mass ejection that increases the storage of mass in a constant volume with a given flattening. Mechanisms (a) and (b) produce a double valued ($\Delta V, \Delta D$) SPh relation, while (c) produces a single valued relation. Only mechanisms (a) and (c) can easily produce the observed amounts of emission ΔV and ΔD without violating the modeling constraints from (i) to (iv) imposed by observations. The model SPh slopes of ($\Delta V, \Delta D$) show the global $\sin i$ and $T_{\rm eff}$ observed dependencies. The scenarios used to describe the double valued ($\Delta V, \Delta D$) suggest another possible way how to build up circumstellar envelopes around Be stars.

Key words: stars: activity – stars: atmospheres – stars: circumstellar matter – stars: emission-line, Be

Send offprint requests to: J. Zorec

1. Introduction

In a recent work, Moujtahid et al. (1998, hereafter MZH) have studied the long-term spectrophotometric (SPh) variations of 49 Be stars using SPh data, photometric magnitudes and colour indices observed over about 50 years. Photometric magnitudes and colour indices collected by different authors in six different photometric systems were homogenized. This enabled us to derive relations between the V magnitude and the $\Phi_{\rm rb}$ (visual gradient of energy distribution) and D (total Balmer discontinuity: BD, $D = D_* + \Delta D$; D_* constant stellar component; ΔD variable circumstellar component) for each program star [gradient $\Phi_{\rm rb}$ and Balmer discontinuity D are defined as in the BCD SPh system (Chalonge & Divan 1952)]. We first sum up the conclusions obtained in MZH and add some results concerning the SPh behaviours obtained by other authors.

1.1. Brief review of results

Line and continuum spectrum variations of Be stars may show some correlation, although not necessarily implying a one to one relation. To avoid possible misunderstandings, in what follows we designate SPh-E the "*spectrophotometric phase of Be stars when the second BD is in emission*: ($\Delta {\rm D} < 0$)", and SPh-A the "*spectrophotometric phase of Be stars when the second BD is in absorption* ($\Delta {\rm D} > 0$)". In the same way, we can also use the designation "SPh-N" for phases where the visible continuum energy distribution of a Be star resembles that of a normal B star, whatever the momentary aspect of the line spectrum. In MZH we could use SPh-Be and SPh-shell respectively for SPh-E and SPh-A. Hence, the main results obtained in MZH may be summed up as follows:

(1) A given Be star, depending on the observing epoch, may be seen in any of the above mentioned SPh phases. Relations between V, $\Phi_{\rm rb}$ and D parameters appear different when they refer to a SPh-E or a SPh-A phase. SPh-E phases are characterized by slopes $\partial(V, \Phi_{\rm rb})/\partial D \neq 0$, positive or negative, depending on the star and epoch: the most frequent combination is $\partial V/\partial D > 0$ (brightening) and $\partial \Phi_{\rm rb}/\partial D < 0$ (reddening) as emission increases ($\partial D < 0$). SPh-A phases more likely show $\partial(V, \Phi_{\rm rb})/\partial D \sim 0$ and $\partial D > 0$. Similar results were

previously obtained by Divan (1979), Divan et al. (1982), Zorec (1986) for a small number of early type Be stars using only BCD data. As all individual SPh variations studied in MZH are published in electronic form[1], we reproduce in Fig. 1a typical SPh-A behaviour observed in HD 37202 and in Fig. 1b that observed in HD 200120 as an example of a SPh-E phase.
(2) Depending on the star, the $(V, \Phi_{\rm rb}, D)$ relations are unique or double valued in a given SPh phase. When they are single, they do not change (or very rarely) after the star has spent some time in another SPh phase.
(3) For most studied stars, the collected observations revealed only one characteristic SPh phase. However, in 8 stars SPh-E $\leftrightarrows$ SPh-A phase changes were detected. Unfortunately, in some Be stars where spectroscopic Be $\leftrightarrows$ shell $\leftrightarrows$ B-normal phase transitions are well known, the scarce photometric data, which are sometimes also heavily marred by errors, did not allow us to study the corresponding SPh behaviour.
(4) SPh-A phases, transitory or more permanent, were detected in some stars with low $V\sin i$ values.

In this context it is worth mentioning the results derived from $uvby$ Strömgren photometry of 13 Be stars by Mennickent et al. (1994), who showed that Be-shell stars have $\partial(b-y)/\partial u \simeq 0$. These authors also found that: (a) the total amplitude of long-term variations is correlated with the average amplitude of short-term variations in each photometric band; (b) there seems to be a correlation between the slope of the (c_1, u) relation and $V\sin i$.

For some stars in typical spectroscopic Be phases, Dachs (1982), Dachs & Hanuschik (1984), Dachs et al. (1988) obtained relations between the V magnitude and the $(B-V)$ colour indices which are characterized by slopes: $-0.34 \lesssim \Delta(B-V)/\Delta V \lesssim -0.1$.

Finally, making use of UBV photometric data spanning about 10 years of a large number of Be stars, it was shown that: (a) brightening is accompanied by reddening in early type Be stars (Hirata & Hubert-Delplace 1981, Hirata 1982), while brightening is correlated with blueing in late type Be stars (Kogure & Hirata 1982); (b) the slope $\Delta V/\Delta(B-V)$ has the same sign as $\Delta(U-B)/\Delta(B-V)$ and the latter is steeper when the $V\sin i$ is higher (Hirata & Hubert-Delplace 1981, Hirata 1982).

1.2. Aim of the present work

The above-mentioned results of MZH refer to a relatively large number of Be stars. So it is worth studying this data, first as a function of fundamental stellar parameters to check the SPh-like correlations obtained in previous works, and then to find new incidences of stellar characteristics on the observed SPh behaviours. We shall also use these data to discuss global properties of CE regions responsible for the observed SPh variations.

[1] CDS via anonymous ftp to cdsarc.u-strasb.fr (130.70.128.5) or http://cdsweb.u-strasb.fr/Abstract.html

2. Correlations with fundamental stellar parameters

In this section we study the correlations between slopes of SPh behaviours obtained in MZH with the following stellar parameters: $V\sin i$, $V_{\rm c}$ (critical equatorial linear velocity of rigid rotation), $T_{\rm eff}$ and $V\sin i/V_{\rm c}$ which is used as an aspect angle indicator (see Sect. 2.3.1). In what follows, the SPh slopes are noted as:

$$\left.\begin{array}{lll} {\rm a_U} = \partial U/\partial D & ; \ {\rm a_V} & = \partial V/\partial D \\ {\rm a_\Phi} = \partial \Phi_{\rm rb}/\partial D & ; \ {\rm a_{\Phi V}} & = \partial \Phi_{\rm rb}/\partial V \end{array}\right\} \quad (1)$$

Units of slopes $\rm a_U$ and $\rm a_V$ are mag dex^{-1}, for $\rm a_\Phi$ μm dex^{-1} and for $\rm a_{\Phi V}$ μm mag^{-1}.

2.1. Data used

For each studied star the slopes $\rm a_U$, $\rm a_V$, $\rm a_\Phi$, $\rm a_{\Phi V}$ and their respective statistical uncertainty are given in Table 1. When Be stars have two slopes corresponding to the same kind of SPh phase, they are both considered separately. The same was also done for a given star when it showed two different SPh phases.

Effective temperatures, radii and masses of our program Be stars were determined from the "photospheric" BD (D_*) and, when available, the BCD λ_1 parameter. For stars without a measured λ_1 parameter, we adopted the mean λ_1 corresponding to its MK luminosity class. Calibrations of (λ_1, D_*) in $T_{\rm eff}$, $M_{\rm bol}$ are from Divan & Zorec (1982), Zorec (1986). With $T_{\rm eff}(\lambda_1, D_*)$ and $M_{\rm bol}(\lambda_1, D_*)$ we determine both the stellar radius $R_*(\lambda_1, D_*)/R_\odot$ and the stellar mass using Maeder & Meynet's (1988) evolutionary tracks. The critical velocity $V_{\rm c}$ is then derived assuming $R_{\rm c} = 1.44 R_*$ (Sackmann 1970, Bodenheimer 1971, Zorec et al. 1988). The $V\sin i$ parameters are mostly from Slettebak (1982) except for HD 37202 (Yang et al. 1990). The stellar parameters used in this work are given in Table 1.

2.2. Results

Instead of considering each SPh slope individually, for they are marred to some extent by uncertainties, we preferred to study mean values of slopes per interval of a given stellar parameter. Mean values are obtained independently for SPh-E and SPh-A phases. In this way, trends indicating possible underlying parametric dependencies can be made conspicuous more clearly. For some stars there are two slopes in a given SPh phase. As in each of them points correspond to different observation epochs, they were considered independently. In the calculation of mean slopes we did not take into account those for which the total detected variation of D was $|\Delta {\rm D}| \lesssim 0.02$. The sampling intervals used are: 50 km s^{-1} for velocities, 0.125 for the velocity ratio $V\sin i/V_{\rm c}$ and 1250 K for the effective temperature. The resulting means, with their respective bars representing 1 standard deviation, are shown in Figs. 2 to 5. In these figures, filled squares are for SPh-E phases and open squares for SPh-A phases.

Results shown in Figs. 2 to 5 can be summed up as follows:

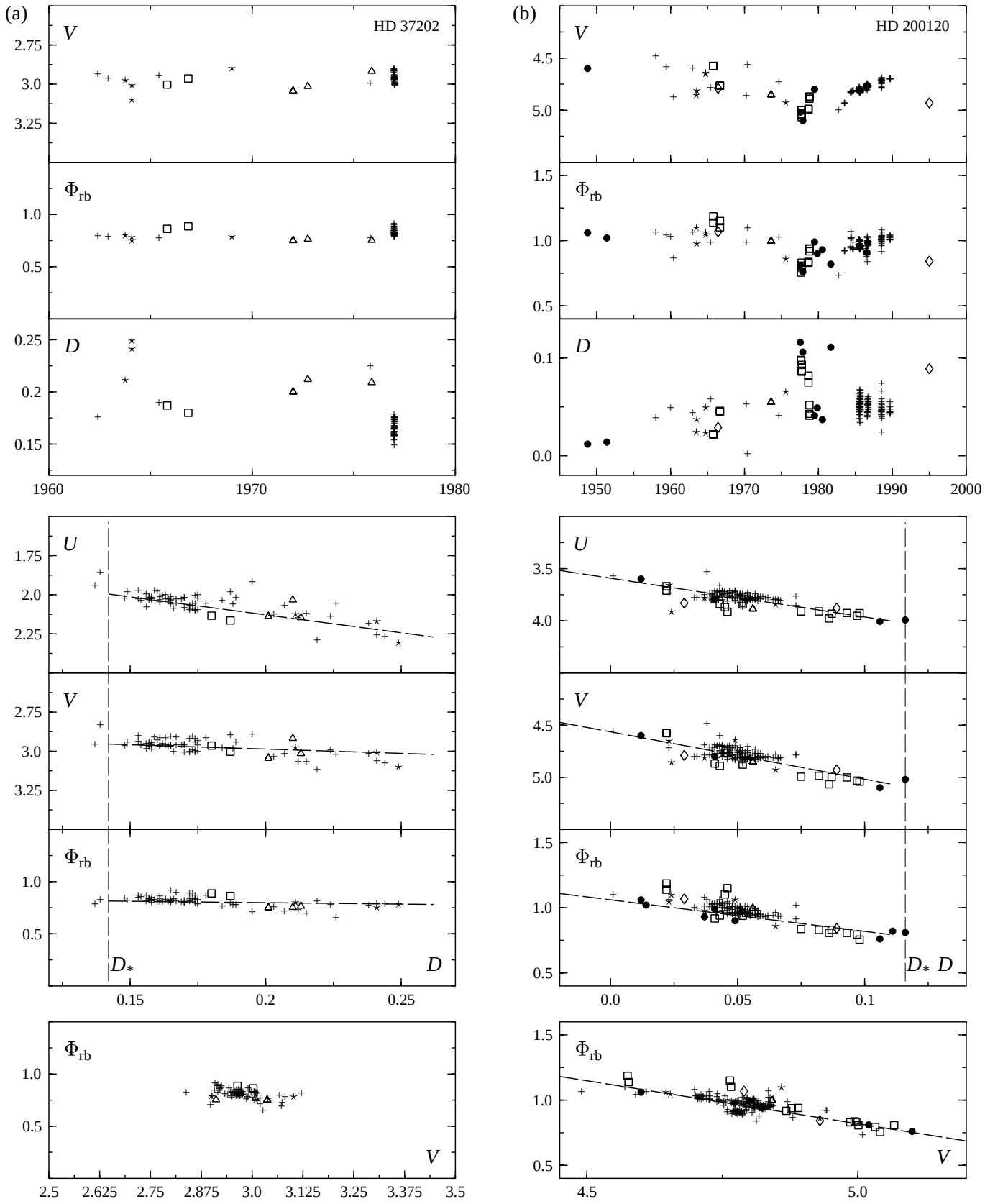

Fig. 1a and b. Spectrophotometric behaviour of Be stars. **a** HD 37202 (SPh-A phase); **b** HD 200120 (SPh-E phase). Symbols are: • BCD data; + UBV data; ⋆ $UBVRI$ data; △ Geneva photometry; ⋄ $uvby$ data; □ 13 colour photometry

Table 1. Fundamental parameters and SPh slopes of the studied Be stars

HD		$V \sin i$	V_c	$\log T_{eff}$	a_U	σ_U	a_V	σ_V	a_Φ	σ_Φ	$a_{\Phi V}$	$\sigma_{\Phi V}$
4180	E	220	300	4.138	4.42	1.92	4.54	1.90	-2.19	0.86	-0.19	0.10
5394	E	230	606	4.519	1.85	0.20	0.27	0.24	-0.45	0.18	-0.25	0.05
	E				2.80	0.32	4.58	0.80	-3.12	0.92	-0.84	0.10
23862	A	320	390	4.067	3.43	0.72	0.85	0.14	0.01	0.04	0.02	0.04
	A				2.03	0.89	-0.51	0.17	0.00	0.03	0.00	0.03
	E				1.72	0.90	1.36	0.13	-0.68	0.15	0.02	0.02
	E				-0.01	0.05	-2.63	0.39	-0.72	0.07	0.01	0.03
24534	E	200	567	4.521	1.03	0.42	4.09	0.58	-2.19	0.25	-0.53	0.05
	E				4.34	0.78	1.39	0.31	-1.05	0.15	-0.20	0.11
	A				0.00	0.51	0.00	0.61	0.00	0.04	0.00	0.046
25940	E	200	401	4.214	1.68	0.74	0.12	0.09	-2.88	0.36	-0.07	0.35
	A				0.24	0.19	0.00	0.53	-2.40	0.37	0.00	0.15
28497	E	230	505	4.455	2.89	0.18	2.09	0.17	-1.26	0.10	-0.46	0.05
32343	E	100	442	4.229	-1.52	0.65	-3.13	0.69	-0.38	0.22	0.00	0.06
33328	E	220	406	4.329	0.63	0.22	0.39	0.18	-1.86	0.14	-0.04	0.05
35439	E	320	426	4.354	2.94	0.20	3.25	0.22	-2.46	0.10	-0.58	0.03
37202	A	320	426	4.325	2.29	0.22	0.20	0.17	-0.21	0.17	-0.05	0.10
37967	E		443	4.229	0.13	0.82	-0.56	0.88	-1.39	0.34	-0.10	0.10
48914	A		180	4.114	2.78	0.15	1.02	0.17	-0.17	0.09	-0.02	0.05
48917	E	200	405	4.329	2.40	0.12	1.95	0.16	-1.64	0.09	-0.51	0.02
50123	E	220	320	4.160	2.39	0.20	0.89	0.28	-0.52	0.32	-0.86	0.05
56014	A	150	335	4.253	3.33	1.07	0.19	0.38	0.00	0.19	0.00	0.11
	E				4.47	0.39	3.35	0.15	0.65	0.10	0.32	0.02
56139	A	80	434	4.333	4.58	0.76	0.24	0.14	-0.36	0.17	-0.22	0.04
	E				2.52	0.55	4.52	0.65	-3.42	0.23	-0.52	0.04
58050	E	140	477	4.346	2.93	0.65	1.60	0.82	-0.69	0.33	-0.31	0.07
58978	E	280	567	4.483	-0.33	0.41	-0.81	0.36	-1.62	0.17	0.10	0.03
60848	E	228	623	4.535	2.29	0.35	2.25	0.45	-2.08	0.29	-0.76	0.11
60855	E	230	420	4.265	1.63	0.86	1.19	0.61	-1.65	0.61	-0.34	0.22
63462	E	320	625	4.483	0.01	0.23	-0.76	0.16	-1.30	0.15	0.34	0.08
65875	A	148	451	4.333	2.16	1.12	0.34	0.27	-0.12	0.07	0.00	0.27
	E				-0.26	0.55	-1.92	0.68	-1.27	0.36	-0.02	0.14
68980	E	115	518	4.452	3.33	0.87	2.82	0.72	-1.62	0.19	-0.32	0.03
	E				-1.07	0.61	-1.02	0.23				
83953	E	260	407	4.177	2.19	0.25	0.65	0.21	-0.47	0.18	-0.23	0.11
89890	A	70	356	4.210	0.55	0.21	0.57	0.16	-0.40	0.17	-0.05	0.12
91120	A	250	343	4.043	2.67	0.44	0.00	0.23	0.00	0.16	0.00	0.14
91465	E	250	337	4.253	1.59	1.71	-1.21	1.22	0.88	0.63	0.35	0.08
109387	E	200	378	4.143	1.11	0.15	-0.33	0.17	-0.58	0.13	-0.44	0.07
120991	E	70	369	4.325	3.06	0.10	2.83	0.12	-1.88	0.04	-0.55	0.02
	E				0.36	0.07	-0.18	0.05	-1.18	0.04	-0.45	0.03
131492	A	100	460	4.279	1.62	0.64	0.51	0.23	-0.13	0.09	0.06	0.03
	E				2.57	1.35	4.50	0.38	-1.38	0.19	-0.27	0.04
142983	A	400	366	4.235	2.67	0.04	0.40	0.09	-0.03	0.01	0.14	0.01
148184	E	140	539	4.455	-1.03	1.09	-1.12	0.31	-2.27	0.15	-0.54	0.05
	E				0.97	0.73	3.83	1.40			-0.60	0.06
162428	E	350	380	4.086	1.98	0.07	0.24	0.14	-0.25	0.18	-0.10	0.03
162732	E	300	376	4.115	2.02	4.40	1.15	2.00	0.12	0.73	0.11	0.07
	A				0.97	0.48	0.13	0.23	-0.19	0.15	-0.03	0.05
168797	E	240	430	4.225	2.68	0.67	1.14	0.35	-0.60	0.23	-0.20	0.07
173219	E		567	4.483	1.18	0.32	0.43	0.24	-1.32	0.20	0.10	0.05
178175	A	120	476	4.346	2.34	0.50	0.00	0.21	0.00	0.28	0.00	0.08
183656	A	300	406	4.139	2.05	0.11	0.09	0.08	-0.25	0.04	-0.03	0.04
184279	A	228	583	4.483	4.45	0.14	2.75	0.10	-0.30	0.07	-0.01	0.02
187811	A	230	470	4.314	2.96	0.59	0.48	0.30	-0.42	0.19	-0.17	0.04
191610	E	320	420	4.265	2.08	0.29	0.47	0.23	-0.39	0.23	-0.10	0.07
195325	A	280	328	4.043	2.44	0.27	-0.11	0.42	0.00	0.19	0.00	0.14

Table 1. (continued)

HD		$V \sin i$	V_c	$\log T_{eff}$	a_U	σ_U	a_V	σ_V	a_Φ	σ_Φ	$a_{\Phi V}$	$\sigma_{\Phi V}$
200120	E	260	512	4.455	3.09	0.23	4.45	0.30	-3.38	0.18	-0.59	0.04
205637	A	250	305	4.255	3.33	0.08	1.53	0.06	-0.25	0.03	-0.07	0.02
210129	E	151	405	4.120	3.06	0.30	1.67	0.34	-0.63	0.06	-0.31	0.04
217050	A	300	370	4.253	2.26	0.07	0.47	0.04	-0.35	0.04	-0.07	0.04
217543	E	370	429	4.247	0.64	0.36	-0.04	0.22	-1.40	0.27	0.22	0.21
218674	A	223	422	4.265	1.19	0.29	0.17	0.08	-0.30	0.12	-0.03	0.07

Note: "E" and "A" in 2nd column stand respectively for SPh-E and SPh-A phases. Units of slopes a_U and a_V and their respective dispersions are mag/dex, for a_Φ and σ_Φ μm/dex and for $a_{\Phi V}$ and $\sigma_{\Phi V}$ $\mu \mathrm{m}/\mathrm{mag}$

(i) We can immediately see that there is a clear distinction between the SPh-E and SPh-A slopes. Excepting mean values of a_U, all remaining averaged slopes corresponding to SPh-A behaviours are $\overline{a}_V \gtrsim 0$, $\overline{a}_\Phi \sim \overline{a}_{\Phi V} \sim 0$. In a number of stars slopes have high intrinsic errors. When $\overline{a} \sim \sigma \sim 0.20$ we can consider that $\overline{a} \sim 0$. Exceptions like HD 184279 definitely have $\overline{a}_V \neq 0$. Other stars in SPh-A phases have $\overline{a}_V \neq 0$ for $\Delta D \lesssim 0.1$ and $\overline{a}_V \sim 0$ for $\Delta D \gtrsim 0.1$.
(ii) T_{eff}-dependence is detected for a_V and a_Φ.
(iii) Correlation with V_c is detected for mean a_V and a_Φ slopes.
(iv) Correlations of slopes against $V \sin i$ and $V \sin i / V_c$ can be considered equivalent. Mean values of a_V and a_Φ slopes correlate with $V \sin i$ and $V \sin i / V_c$.
(v) No clear correlations with any of studied stellar parameters seem to be outstanding for the mean a_U slopes.

For easy comparison of the present results with previous results dealing with SPh behaviours, we reproduce the regression lines of mean slopes $\overline{a}_V$, $\overline{a}_\Phi$, $\overline{a}_{\Phi V}$ which can be used simply as indications for possible mean dependencies on the respective stellar parameters. Regression lines for SPh-E phases are:

$$\left.\begin{array}{rcl} \overline{a}_V & \sim & -(0.010 \pm 0.002) V \sin i + (3.3 \pm 0.6) \\ \overline{a}_\Phi & \sim & (0.005 \pm 0.001) V \sin i - (2.3 \pm 0.2) \\ \overline{a}_{\Phi V} & \sim & (0.002 \pm 0.001) V \sin i - (0.5 \pm 0.2) \end{array}\right\} \quad (2)$$

$$\left.\begin{array}{rcl} \overline{a}_V & \sim & -(1.8 \pm 0.3)(V \sin i / V_c) + (2.3 \pm 0.2) \\ \overline{a}_\Phi & \sim & (1.9 \pm 0.3)(V \sin i / V_c) - (2.4 \pm 0.3) \\ \overline{a}_{\Phi V} & \sim & (0.44 \pm 0.04)(V \sin i / V_c) - (0.51 \pm 0.03) \end{array}\right\} \quad (3)$$

$$\left.\begin{array}{rcl} \overline{a}_V & \sim & (0.007 \pm 0.002) V_c - (1.8 \pm 0.7) \\ \overline{a}_\Phi & \sim & -(0.006 \pm 0.001) V_c + (1.5 \pm 0.5) \\ \overline{a}_{\Phi V} & \sim & -(0.001 \pm 0.001) V_c + (0.0 \pm 0.1) \end{array}\right\} \quad (4)$$

$$\left.\begin{array}{rcl} \overline{a}_V & \sim & (1.4 \pm 0.5 (T_{eff}/10^4) - (1.8 \pm 1.1) \\ \overline{a}_\Phi & \sim & -(0.6 \pm 0.5)(T_{eff}/10^4) - (0.0 \pm 0.3) \\ \overline{a}_{\Phi V} & \sim & -(0.02 \pm 0.10 (T_{eff}/10^4) - (0.2 \pm 0.3) \end{array}\right\} \quad (5)$$

The significance level of SPh-A mean slope regressions are too low to suggest any reliable correlation. The values of mean SPh-A slopes scatter near zero and are characterized by the following averages and 1σ dispersions:

$$\left.\begin{array}{rcl} \overline{a}_V & = & 0.44 \pm 0.55 \\ \overline{a}_\Phi & = & -0.21 \pm 0.20 \\ \overline{a}_{\Phi V} & = & -0.02 \pm 0.05 \end{array}\right\} \quad (6)$$

Comparing our results with those obtained in previous works, we observe that:

(a) Slopes $\overline{a}_\Phi \lesssim 0$ in SPh-E phases, which suggests that, as a mean, there is reddening of visible energy distribution as emission in the second BD increases. Nevertheless, two exceptions (HD 56014 and HD 91465) have been found that present some blueing as emission increases in the second BD;
(b) Similarly to the findings of other authors, slopes $\overline{a}_V \gtrsim 0$ in SPh-E phases, which corresponds to brightening in the V magnitude as the continuum Balmer emission is higher. Increased faintness in the V magnitude as emission in the second BD increases was however found in HD 32343, HD 68980 (during one of its SPh-E periods) and in HD 148184 during its period of strongest emission. For HD 148184, Dachs (1982) reports lowering of Hα line emission from 1972 to 1979, when the star showed brightening in the V magnitude;
(c) Comparing our results with those of Hirata (1982) and Hirata & Hubert-Delplace (1981), we see that reddening of the visible energy distribution in SPh-E phases implied by a_Φ in relations (5) or in Fig. 5 is smaller for lower effective temperatures, but that it never turns to a blueing effect for lower temperatures, as noted in Kogure & Hirata (1982). We note that blueings of photometric indices can sometimes be due to variable spectral lines produced in CE, so that they do not necessarily correspond to a temperature effect;
(d) Using the transformations from UBV photometric to SPh indices obtained in MZH [cf. (1), (2) and (3)], we readily derive the following relations between photometric and SPh slopes:

$$\Delta V / \Delta (B - V) = 0.56 / a_{\Phi V} \quad (7)$$

$$\Delta (U - B) / \Delta (B - V) = (3.55 / a_\Phi) + 0.67 \quad (8)$$

which allow us to compare the photometric results discussed by other authors with the SPh results used in the present work. Using the $a_{\Phi V}$ and a_Φ slopes listed in Table 1 respectively in (7) and (8), we confirm the results previously obtained by Hirata (1982) and Hirata & Hubert-Delplace (1981), where it was noted that in SPh-E phases $\Delta V / \Delta (B-V)$ and $\Delta (U-B) / \Delta (B-V)$ have the same sign. However, we have found some exceptions to these rules which are observed in HD 58978, HD 63462, HD 173219 and HD 217543;
(e) Introducing relation (2) for a_Φ into (8), we see that $\Delta (U - B) / \Delta (B - V)$ is steeper when $V \sin i$ is higher as also claimed

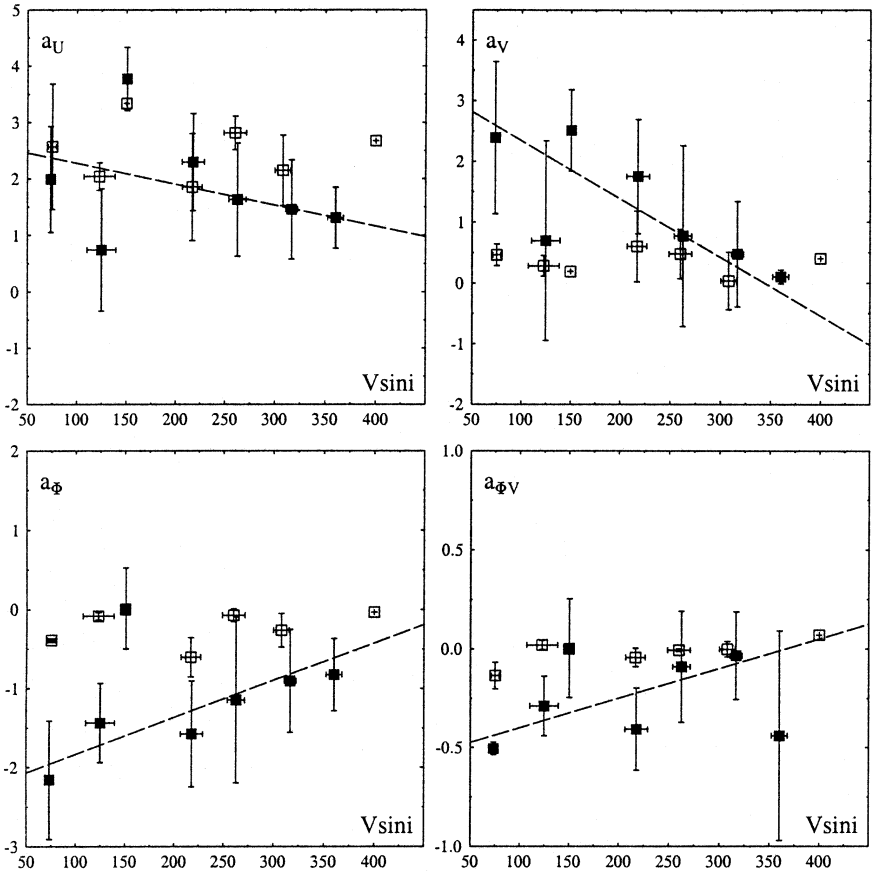

Fig. 2. Averaged SPh slopes a_U, a_V, a_Φ and $a_{\Phi V}$ against $V \sin i$. "Filled squares" for SPh-E phase; "open squares" for SPh-A phase. Regression lines shown refer to SPh-E phases only.

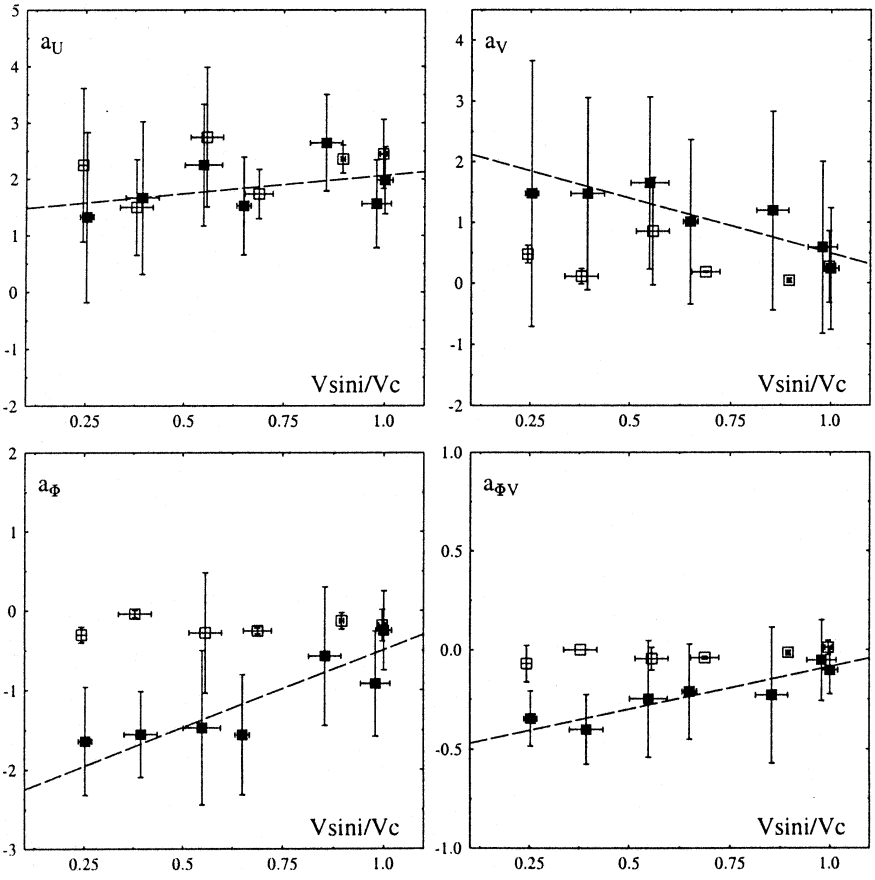

Fig. 3. Idem Fig. 2 but against $V \sin i / V_c$

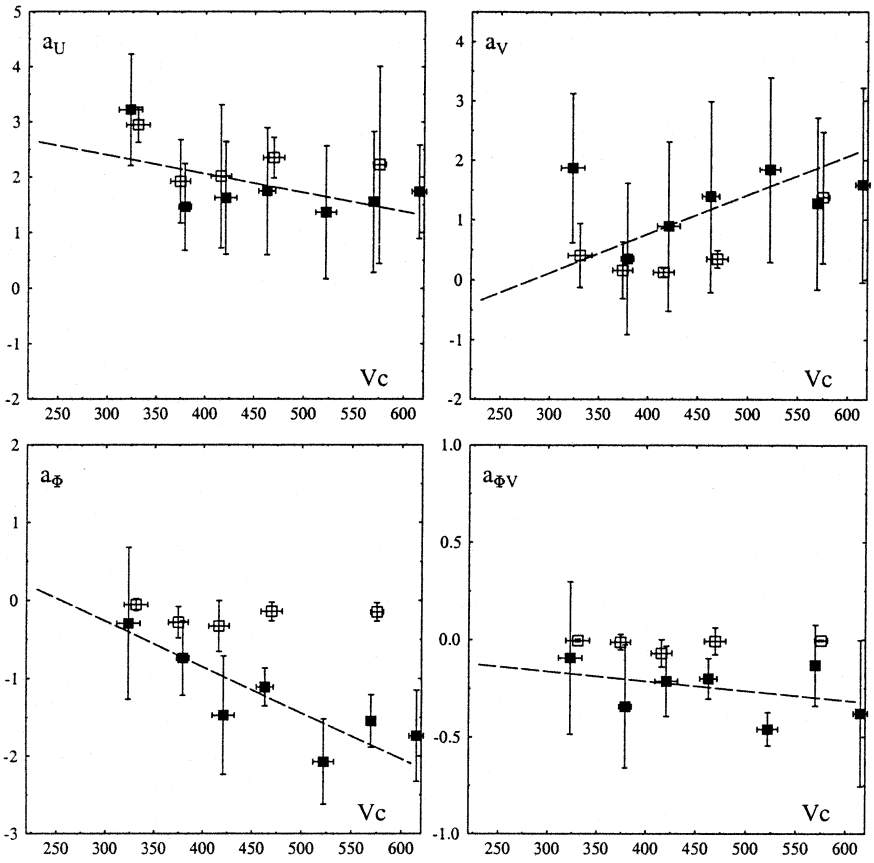

Fig. 4. Idem Fig. 2 but against V_c

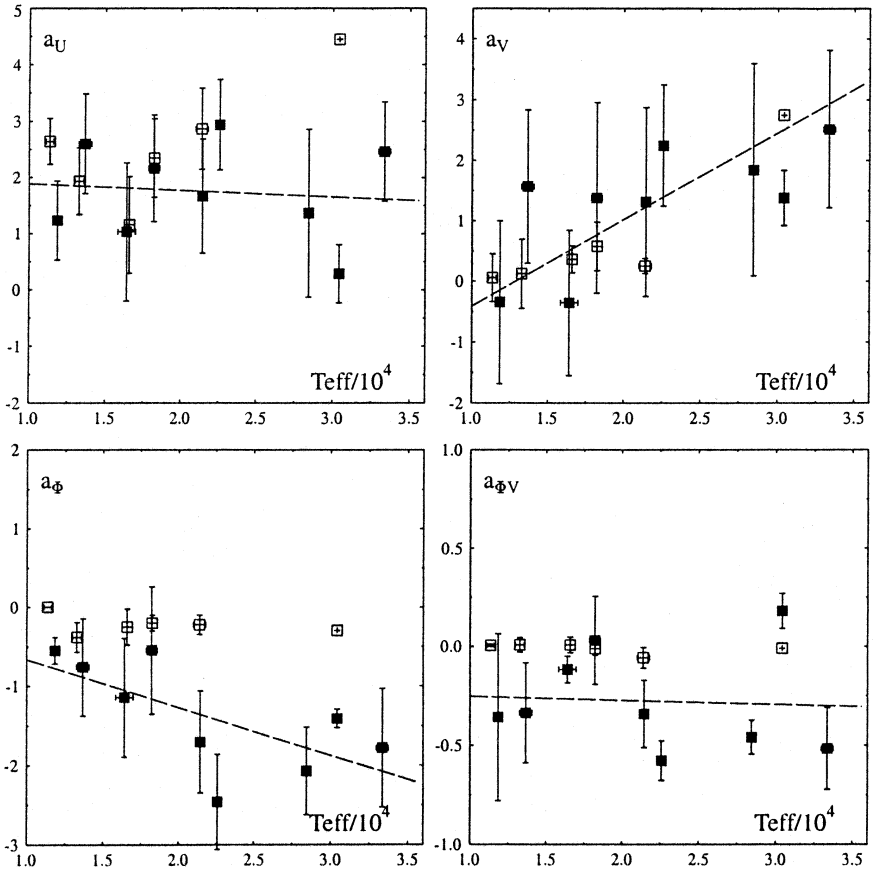

Fig. 5. Idem Fig. 2 but against T_{eff}

in previous works. Using now relation (5) for a_Φ in (8), we can still add that $\Delta(U-B)/\Delta(B-V)$ is flatter when $T_{\rm eff}$ is higher; (f) Dachs et al. (1988) found that the ratio $\Delta(B-V)/\Delta V \gtrsim -0.34$. They also found that absolute values of this slope are twice as small as those predicted theoretically. Using the $a_{\Phi V}$ slopes given in Table 1, we find that in SPh-E phases this ratio not only has negative values as low as $\Delta(B-V)/\Delta V \gtrsim -2$, but that it can also have positive values $\Delta(B-V)/\Delta V \lesssim 0.6$ as previously also noted by Hirata (1982).

2.3. Correlations of SPh parameters with stellar parameters

Noticeable correlations seem to exist for mean a_V and a_Φ SPh slopes with $V\sin i$ (and/or $V\sin i/V_c$), V_c and $T_{\rm eff}$. A correlation between V_c and $T_{\rm eff}$ is not expected in a sample where stars are of different luminosity classes. Nevertheless, the regression line obtained for stars in the SPh-E phase: $\log V_c = (0.04 \pm 0.45) + (0.61 \pm 0.10) \log T_{\rm eff}$ is obtained with a correlation coefficient $r = 0.84$. On the other hand, $\log V_c = (-0.24 \pm 0.17) + (0.67 \pm 0.04) \log T_{\rm eff}$ with $r = 0.95$ is derived by using the mean values of V_c and $T_{\rm eff}$ corresponding to the sampling intervals of Figs. 4 and 5. This shows that mixing of luminosity classes in our sample is not high enough to prevent a rather clear relation between V_c and $T_{\rm eff}$. This also means that correlations of a_V and a_Φ against V_c and $T_{\rm eff}$ can be considered synonymous.

2.3.1. Correlations with $V\sin i$ and/or $V\sin i/V_c$

We have just seen that for our program stars there is a well defined relation between V_c and $T_{\rm eff}$. On the other, as we shall see, the "true" rotational velocity V of Be stars can be considered nearly proportional to V_c. So, this could imply that trends in Figs. 2 and 3 might be considered to be due to some temperature effect. However, the following argument supports the assumption of a dominant aspect angle effect.

Distributions of the angular velocity ratio $\omega = \Omega/\Omega_c$ (Ω_c critical angular velocity for rigid rotation) of Be stars are strongly peaked, according to the spectral type and luminosity class, from $\omega \simeq 0.7$ to $\omega \gtrsim 0.8$ (Zorec 1986, Zorec & Briot 1997). In Fig. 6 is shown the distribution of the most numerous group of Be stars: B2+B2.5+B3 main sequence stars, obtained from their observed distribution of $V\sin i$ (histogram) and corrected from errors in $V\sin i$ (Smart 1958) and random distribution of the inclination i (Lucy 1974). It can be seen that 80% of these stars are rotating in the $0.60 < \omega < 0.95$ interval. The distribution of true rotational velocities of Be stars of all subspectral types together (Porter 1996) also has the same appearance as the one for the B2+B2.5+B3 main sequence stars. We can then safely assume that the value $\overline{\omega} = 0.8$ represents a reliable approach to the mean probable value of ω at which the Be stars rotate. Slettebak et al. (1992) used $\overline{\omega} = 0.9$. Thus, to infer the probable viewing angle of Be stars we shall use the interval $\omega = 0.80 \pm 0.15$ (Sect. 3.1), so that $\sin i = 1.55 V\sin i/V_c$ [we used $R_*(\omega)/R_c \simeq 0.69 + 0.0024 e^{4.86\omega}$ for the equatorial radius deformed by rigid rotation (Sackmann 1970, Bodenheimer 1971, Zorec et al. 1988)]. As the mean value of V_c in each sampling interval of $V\sin i$ of Figs. 2 and 3 is amazingly the same: $450 \pm 50\,{\rm km\,s^{-1}}$, it means that trends shown in Figs. 2 and 3 are due to a genuine aspect angle effect. The high dispersion of points in Figs. 2 and 3 is not only due to measurement uncertainties of SPh slopes, but also to possible physical phenomena which are discussed in Sect. 3.3.

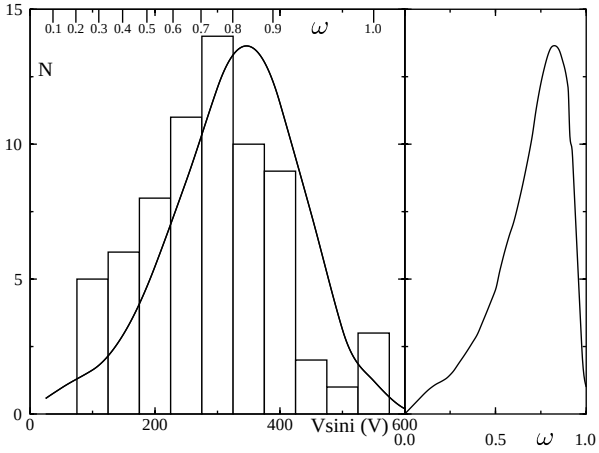

Fig. 6. Distribution of B2+B2.5+B3 main sequence Be stars against rotational velocities $V\sin i$, V and $\omega = \Omega/\Omega_c$

2.3.2. Correlations with $T_{\rm eff}$

The visible continuum emission is proportional to the emission measure. The latter is larger when the radius of the H-ionized region is more extended, so when $T_{\rm eff}$ is higher. It is expected then that SPh variations will also be more noticeable if stars are hotter. Such a tendency is depicted by the trends in Fig. 5 of a_V and a_Φ SPh slopes against $T_{\rm eff}$.

3. Interpretation of SPh variations

3.1. Constraints for CE models

In the preceding section we have shown that mean a_V and a_Φ give insights for mean aspect angle and temperature dependencies. However, from star to star the CE regions near the central star responsible for the observed SPh behaviours can have a variety of geometric and physical structures. At the moment, we would like to investigate only the most outstanding characteristics of these regions using simple but sufficiently general CE models: (a) to estimate the first order effects produced on the visible spectrum by different geometrical structures of CE (discs, ellipsoids); (b) to draw out easily global statistical conclusions. To do so, we shall first quote some relevant characteristics that must be respected by any CE model to ensure basic consistencies with observations.

(a) – *On the extent of CE regions producing the SPh changes*

Interferometric measurements of γ Cas (Stee et al. 1998) show that the diameter of the CE zone producing the continuum flux excess in $\lambda \sim 0.65$ μm at the observing epoch is $3.5R_*$ and

$2.8R_*$ for $\lambda \sim 0.48$ μm. It is then expected that the radius of the region forming the continuum radiation at $\lambda \sim 0.56$ μm will not exceed $1.6R_*$. The bulk of visible continuum radiation was predicted by Poeckert & Marlborough's disc CE model for γ Cas to originate from within twice the observed extent: $3R_*$. In general, as radiation in the visible continuum is dominated by H recombination and by stellar light scattered by free electrons, the studied CE region must be rather highly ionized. H ionization proceeds efficiently from the second level (Höflich 1988, Millar & Marlborough 1998). So, the volume of the visible continuum formation region should be proportional to the generation rate of stellar Balmer photons (Osterbrock 1989): $Q_{\rm Ba} = \int_{\nu_{\rm Ba}}^{\infty}(L_\nu/h\nu)d\nu \propto R_*^2 T_{\rm Ba}^3 \propto R_{HII}^3 N_{\rm H}^2$ ($T_{\rm Ba}$ = mean temperature of stellar layers supplying the Balmer photons). Thus, the expected range of CE zone radii $R \simeq 2.33(T_{\rm Ba}/10^4)(R_*/R_\odot)^{-1/3}(N_H/10^{12})^{-2/3}$, assuming $N_H \sim 10^{12}$ cm^{-3}, is $1.2R_*$(B9V) $\lesssim R \lesssim 1.9R_*$(B0V) in close agreeemnt with observations of γ Cas. This suggests that CE zones contributing to the observed magnitude V are very near the central star: *about or less than 2 stellar radii*.

(**b**) – *On the density of CE regions implied by the SPh changes*

Among the most noticeable characteristics of SPh variations is the appearance and variation of the second component of the BD. This component is either in emission (SPh-E phases), or in absorption (SPh-A phases) (Barbier & Chalonge 1939, 1941, Divan 1979, Zorec & Briot 1991). The emission rise (or the absorption fall) of the second BD begins closely at $\lambda \lesssim 3670$ Å in almost all Be stars. This emission (or absorption) reaches its highest value at $\lambda \simeq 3647$ Å. Excepting some rare and short lasting cases, no coninuum emission rise (or absorption fall) is noticeable from $\lambda 3680$ to $\lambda 3700$. Using the Vidal's (1966) relation, or simply the known Inglis-Teller formula, this wavelength limit implies that there can be an upper limit to the CE base density at about $N_{\rm e}^* \lesssim 10^{13}$ cm^{-3}. We note that emission intensities in Hα, Hβ, Hγ lines and that in the visible continuum of some Be stars have been consistently explained by Höflich (1988) using spherical CE with base densities $N_{\rm e}^* \lesssim 10^{12}$ cm^{-3}.

(**c**) – *SPh phases vs. aspect angle of Be stars*

We note that some program Be stars, with aspect angles probably $i \lesssim 50^o$, have shown widely recorded spectroscopic Be-shell phases which also unavoidably imply strong differences $\Delta D > 0$. However, simultaneous photometric observations in both sides of the BD were curiously not carried out during their phase changes. Among these stars, the most significant are HD 5394 (Underhill & Doazan 1982) and HD 200120 (Hubert-Delplace & Hubert 1981, Underhill & Doazan 1982). Concerning HD 200120, a decrease of more than 1 mag in the far-UV energy distribution was observed with the TD-1 satellite (Beeckmans 1976) during one of its spectroscopic Be-shell phases (1972-mid 1974). Hummel (1998) explains the line variations during these rather short lasting phase changes with a temporarily tilted circumstellar disc. The photometric behaviour in these phases can also be explained in terms of huge prominence-like ejections (Zorec et al. 1999). However, in our sample there are a number of Be stars with rather low $\sin i$, which are seen in long duration spectroscopic Be-shell and SPh-A phases: HD 56014, HD 184279, HD 187811 and HD 218674. On the other hand, Be stars not included in our sample have shown strong shell characteristics in their spectra, like HD 45542 ($V \sin i = 170$ km s^{-1}) (Hanuschik et al. 1996). According to the discussion in Sect. 2.3.1, the expected mean aspect angle of this group of stars is small: $< i^o > \simeq 45^{+21}_{-16}$ (upper inclination for $\omega = 0.65$; lower inclination for $\omega = 0.95$; mean dispersion of means $\sigma = 11^o$).

Contrary to the preceding situation, where Be stars with low $\sin i$ seen at SPh-A phases, there are Be stars with $\sin i \sim 1$, which are more frequently seen as Be-shell and SPh-A, but which have shown long lasting Be and SPh-E phases. The best known is Pleione (HD 23862), for which there is a vast literature about its phase variations (Hirata & Kogure 1976, Gulliver 1977). This star is seen nearly equator-on: $i \simeq 90^o$. On the other hand, stars like HD 4180, HD 35439, HD 83953, HD 91465, HD 162428, HD 191610 and HD 217543 which are more or less in genuine spectroscopic Be and SPh-E phases have a mean probable inclination $< i^o > \simeq 71^{+19}_{-19}$ (lower limit of inclination for $\omega = 1.0$; upper limit of inclination for average value of maximum attainable ω of these stars $\overline{\omega}_{\rm max} = 0.88 \pm 0.06$; mean dispersion of means $\sigma = 12^o$). In these stars spectroscopic Be-shell and SPh-A phases are rare and weak, or they have not yet been seen (Hubert-Delplace & Hubert 1979). In the frame of flattened CE models, such as those of Poeckert & Marlborough (1978a,b), these objects must all be seen at low inclinations [$i \lesssim 45^o$, also see (**f**)].

Though it would not be impossible to account for SPh-E $\leftrightarrows$ SPh-N $\leftrightarrows$ SPh-A changes when $i < \pi/2 - \Delta\theta$ ($\Delta\theta$ half-opening angle of CE) with flattened CE, SPh-A phases cannot be produced with them if $i < \pi/2 - \Delta\theta$. Hence, a great number of Be stars, far from being an exception, seem to be seen at inappropriate angles in regard to predictions of strongly flattened CE models.

(**d**) – *Interferometric data and the aspect angles*

Interferometric measurements of Be stars (Quirrenbach et al. 1993, 1994, 1997; Stee et al. 1995, Stee et al. 1998) were done for the following Be stars: HD 5394, HD 10516, HD 22192, HD 23630, HD 25940, HD 37202. The apparent ellipticities E_{app} of the Hα emission line formation regions in the respective CE, aspect angles i_ω^o calculated as discussed in Sect. 2.3.1 and the lower limits predicted from $i_{E_{app}} > \arccos E_{app}$ are given in Table 2. We also reproduce the adopted stellar parameters. HD 10516, an interacting binary whose shell appears twice per orbital cycle, was excluded from this table.

From Table 2, taking into account the possible uncertainties in $V \sin i$ and $V_{\rm c}$, we can see that the predicted aspect angles i_ω and $i_{E_{app}}$ do not contradict each other, though $i_{E_{app}}$ is not a genuine measured parameter. HD 23630 and HD 25940 are sometimes considered as slightly hotter than the BCD classifi-

Table 2. Measured CE ellipticities and probable aspect angles of Be stars

HD	Sp.T	$V \sin i$ km s^{-1}	V_c km s^{-1}	E_{app}	i^o_ω	$i^o_{E_{app}}$
5394	O9V	230	606	0.70	36^{+16}_{-11}	> 46
22192	B4III-IV	280	352	0.47	64^{+26}_{-10}	> 62
23630	B8III	140	284	0.95	50^{+13}_{-20}	> 18
25940	B4IV	200	401	0.89	51^{+13}_{-21}	> 27
37202	B2III	320	426	0.28	71^{+19}_{-20}	> 74

Note: We used BCD spectral classification; V_c was derived from (λ_1, D) calibrations in stellar parameters

cation. This leads to a lower estimate of their i_ω. On the other hand, the Hα emission line profiles of these stars are bottle-shaped, which means that their markedly pole-on aspect may be due to non-coherent scattering in the CE (Hummel & Dachs 1992). Hence, they do not necessarily correspond to stars seen at very low aspect angles $i \lesssim 30^o$. Nevertheless, E_{app} is systematically higher and i is lower when stars are in a Be phase, which favors interpretion of observations in terms of flattened CE. We have however shown in (**c**) that there is an important fraction of Be stars where spectroscopic and SPh phases do not obey the phase-aspect angle tendency which would be expected if only discs or strongly flattened CE existed.

(**e**) – *Linear polarization of visual continuum radiation*

Assuming that Be CE envelopes are Thomson scattering dominated axial-symmetric ellipsoids with ellipticity E, a power-law $N_e(R) = N^*_e(R_*/R)^n$ electron density distribution and an extended central source of unpolarized light, using a Monte Carlo method for a multi-scattering approach, it was possible to show that a given linear polarization in the V magnitude in Be stars may correspond to two different optical depths and that observations are consistent on average with $\tau_e \lesssim 1$ and $E \sim 0.7$ (Höflich & Zorec 1989, Höflich et al. 1989, Höflich 1991). We shall see in Sect. 3.3.1 that $\tau_e \lesssim 1$ carry $N^*_e \lesssim 5 \times 10^{12}$ which implies that moderate densities and flattenings of CE may explain the observed polarization in V.

Among the most detailed spectropolarimetric calculations for Be stars are those of Poeckert & Marlborough (1978a) done for γ Cas (HD 5394), and of Wood et al. (1997) for ζ Tau (HD 37202). Shortcomings of Poeckert & Marlborough's attempts were discussed in the work of Wood's et al. It is thus worth commenting the model of ζ Tau, because of its connection with the SPh studied in the present paper. The model is characterized by a thin CE with a half-opening angle $\Delta\theta \simeq 2.5^o$, constant temperature, density distribution $N_e(R) = N^*_e(R_*/R)^3$ with $N^*_e \sim 3.0/\sigma R_* \gtrsim 10^{13}$ cm^{-3} and inclination $i \simeq 82^o$. The model accounts for the BD polarimetric jump, visible and IR spectropolarimetric distributions. It indeed fails to describe the polarimetric distribution in the Balmer continuum and the energy distribution around the BD. In fact, SPh BCD observations spanning about 50 years of ζ Tau have always shown two well defined BD components: (a) a constant photospheric component $D_* = 0.142 \pm 0.010$ dex; $\lambda_1 - 3700 = 44 \pm 1$ Å, so that from Chalonge & Divan's (1973) (λ_1, D_*) calibration into MK classification, the spectral type of ζ Tau is B2III; (b) a variable second component in **absorption** $d = +0.06 \pm 0.05$ dex. Wood's et al. thin CE predicts however a second BD in **emission**. On the other hand, due to the very sudden fall of the second BD at $\lambda \simeq 3660$, the expected electron density at the base of the CE should be nearly an order of magnitude lower than that used in Wood's et al. model. This shows that the thin CE model (Bjorkman & Cassinelli 1993, Owocki et al. 1994) is probably not suitable to explain the visible and near UV energy distribution of ζ Tau. We still note that the wind-compressed disc formation can be inhibited by radiation pressure and rotation (Owocki et al. 1996).

(**f**) – *Visual emission from flattened CE*

Waters & Marlborough (1994) and van Kerkwijk et al. (1995) have discussed difficulties in explaining with disc-like CE models (Waters 1986, Poeckert & Marlborough 1978a) the observed correlations in Be stars between Hα emission and $(J-L)$ colour excess. Regarding the SPh aspects, flattened CE models worked out in detail by Poeckert & Marlborough (1978a,b) show that continuum emission becomes detectable only when $i \lesssim 45^o$ and $N^*_e \gtrsim 10^{13.3}$ cm^{-3}, which conflicts with the density limits discussed in (**b**). For other inclinations and whatever the density, these models always produce continuum absorption ($\Delta V > 0$). Hence, the main difficulty of such models lies in the fact that for low inclinations ($i < \pi/2 - \Delta\theta$) the SPh-E $\leftrightarrows$ SPh-N $\leftrightarrows$ SPh-A cannot be produced by them, and that for $i > \pi/2 - \Delta\theta$ the model fails to produce the SPh-E aspects.

3.2. The model

Taking into account the arguments developed in the preceding subsection, we must be able to explain the observed SPh variations with CE models: (a) where densities do not exceed $N_e \sim 10^{13}$ cm^{-3}; (b) with regions producing the visible continuum which are not greater than some R_*; (c) which easily produce SPh-A and SPh-E phases and variations from one to another, whatever the aspect angle; (d) that explain the bivalued SPh relations [Sect. 1.1(2)]. As we have already noted, strongly flattened CE cannot fulfill requirement (c). Mass loss in Be stars is a strongly variable phenomenon. In addition, these stars show light outbursts which imply short lasting but strong mass ejections (Hubert et al. 1997, Hubert & Floquet 1998). SPh variations are then probably a consequence of dynamic phenomena taking place in the CE. Calculation of SPh variations as a function of these phenomena is outside the scope of this paper. We shall however take them into account in a simplified way using axi-symmetrical CE by varying their extent, base density and/or their flattening (ellipticity).

3.2.1. Electron density distribution in the CE emitting region

The electron density distribution in a disc-like CE is currently represented in the literature by a power-law $N_{\rm e}(R) = N_{\rm e}^*(\frac{R_*}{R})^n$ with $2 \lesssim n \lesssim 3.5$ (Štefl 1998). In the present work we generalize this law by assuming that the electron density is constant over ellipsoidal surfaces, which all have the same ellipticity E. Such a particle density distribution is not far from some theoretical predictions for CE in Be stars (Araújo & Freitas Pacheco 1989, Stee & Araújo 1994, Stee et al. 1995). Making the conservative assumption $n = 2$, the electron density over ellipsoidal CE isopicnic surfaces is then given by $N_{\rm e}(R_{\rm p}) = N_{\rm e}^*(R_*/R_{\rm p})^2$, where $R_{\rm p} = z^2 + E^2(x^2 + y^2)$ is the polar radius of an ellipsoidal surface; x and y are coordinates in the equatorial plane and z is measured from the equatorial plane); $N_{\rm e}^*$ is the base density.

As in what follows an equivalent slab will represent the effect of radiation resulting from an ellipsoidal structure of the CE, its effective aspect angle dependent opacity is assumed to be represented by the one calculated in the radial direction of the viewing angle i. It is then given by (MZH):

$$\left.\begin{array}{rcl} \tau_\lambda & = & \tau_\lambda^p/\Lambda(E,i) \\ \Lambda(E,i) & = & [1-(1-E^2)\sin^2 i]^{1/2} \end{array}\right\} \quad (9)$$

where τ_λ^p is the total [scattering ($\tau_{\rm e}$) + absorption bound-free+free-free (τ^λ)] radial optical depth of the CE in the polar direction. Although this representation looks oversimplified, we shall see that it is able to account for the main angle dependent characteristics of the radition field emerging from the star-CE system.

Some SPh variations studied in Sect. 3.3.2 are for CE which preserve their mass while they change their volume. In CE with constant mass and changing volume, where the index n is constant, the main variation of τ_λ^p is produced by the subsequent drop of the density at the base of the CE. The analytic expressions for τ_λ^p are cumbersome and depend on the configuration whether the CE covers or not the polar regions of the central star. For shortness, if we use power representations $R^{\rm q}$ for the R dependence, τ_λ^p can be approximated to a sufficient degree of accuracy by:

$$\tau_\lambda^p = \tau_\lambda^o \frac{1}{\Lambda(E,i)} (\frac{R_*}{R_{\rm e}})^s f_{\rm e,a}(R_{\rm e}, i, E) \quad (10)$$

All values of s and $f_{\rm e,a}$ ("e" stands for electron scattering and "a" for bb+ff absorption) studied in this paper are between those of to two limiting cases: spherical CE and flat discs. Hence, the scattering component of the total opacity $\tau_{\rm e}^p$has: $s = 1$ for spherical CE and $s = 1.4$ for discs; $f_{\rm e} = 1$ for both cases. The absorption (bf+ff) component $(\tau^\lambda)^p$ has: $s = 2.6$ (spherical CE); $s = 3$ (disc) and $f_{\rm a} = 1$ for both. $\Lambda = 1$ for spherical CE and $\Lambda = \cos i$ for discs.

3.2.2. The radiation field

For a given radial-dependent particle distribution in an ellipsoidal CE, in a good first order approximation, radiation transfer can be reduced to an addition of emitting/absorbing equivalent thin slabs. Neglecting second order effects due to tangential optical depths and assuming isothermal slabs, the emitted radiation flux of a star-CE system like the one depicted in Fig. 7 is given by:

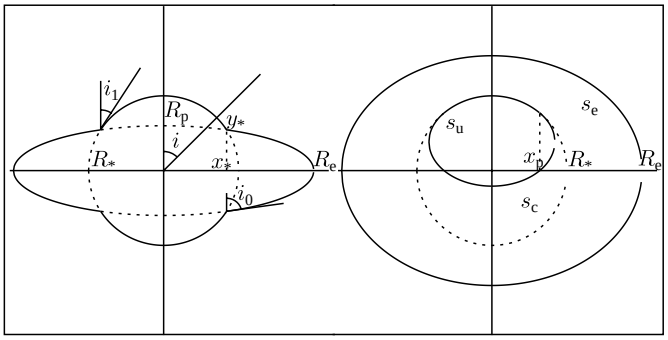

Fig. 7. Geometric elements of the star-CE system ($E = 0.3$; $R_{\rm e} = 2$). Star-CE system observed equator-on (left); Star-CE system projected on the plane perpendicular to the line of sight (right; $i = 45^o$).

$$\frac{F_\lambda}{F_\lambda^*} = s_{\rm u}(R_{\rm e},E,i) + s_{\rm c}(R_{\rm e},E,i)\Big[e^{-\tau_\lambda} + \frac{S_\lambda}{F_\lambda^*}(1-e^{-\tau_\lambda})\Big] + s_{\rm e}(R_{\rm e},E,i)\frac{S_\lambda}{F_\lambda^*}(1-e^{-2\tau_\lambda}) \quad (11)$$

The first term accounts for the energy emitted by the fraction of stellar surface which is not covered by the CE. The second term represents the fraction of stellar energy absorbed by the CE layers between the star and the observer and the energy emitted by the same layers. The third term gives the amount of energy emitted by the CE layers beyond the stellar surface. $s_{\rm u}$ is the fraction of the uncovered stellar surface seen by the observer and projected on the plane perpendicular to the line of sight. $s_{\rm c}$ is the fraction of stellar surface eclipsed by the CE. $s_{\rm e}$ is the area, projected on the background, of the ellipsoidal CE which does not eclipse the star. All quantities $s_{\rm u}$, $s_{\rm c}$ and $s_{\rm e}$ are given in units of the stellar disc area (πR_*^2) and their explicit forms for several inclination intervals are given in Appendix A. The relevant parameters needed to represent the fractional surfaces are shown in Fig. 7. We still have in (11): F_λ^*, the stellar photospheric flux and $R_{\rm e}$, the equatorial radius of the equivalent ellipsoidal shell representing the CE.

Due to electron densities expected in hydrogenic CE of Be stars, opacity due to electron scattering can be significant (Hirata & Kogure 1984, Millar & Marlborough 1998). The scattered radiation field then has to be taken into account in the source function S_λ of the emitting shells (here 'shell' has the literal meaning) (Mihalas 1978):

$$S_\lambda = (1-\epsilon_\lambda)B_\lambda(T) + \epsilon_\lambda J_\lambda \quad (12)$$

where $\epsilon_\lambda = \kappa_{\rm e}/(\kappa_{\rm e} + \kappa_{\rm bf+ff}^\lambda)$ is the ratio of scattering to the total absorption coefficient, B_λ is the Planck function and J_λ is the local mean radiation field, which based on the assumptions used for (11) is given by (Moujtahid 1998):

$$J_\lambda = S_\lambda\Big[1 - e^{-2\tau_\lambda} + \frac{\mu_o}{2}e^{-2\frac{\tau_\lambda}{\mu_o}}\Big(1 - e^{-2\frac{\tau_\lambda}{\mu_o}}\Big)\Big] +$$

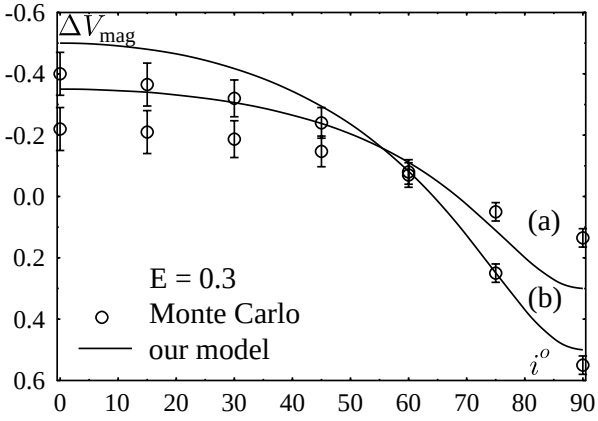

Fig. 8. ΔV magnitude differences for a CE with $E = 0.3$ against i calculated with (11) (full lines) and from a Monte Carlo simulation (open dots) for two base densitites. (a): $N_{\rm e}^* = 2.5 \times 10^{12}$; (b): $N_{\rm e}^* = 5.8 \times 10^{12}\,{\rm cm}^{-3}$

$$\frac{1}{2}F_\lambda^* e^{-2\tau_\lambda}\left[1-\mu_o e^{-2\tau_\lambda(\frac{1}{\mu_o}-1)}\right] \qquad (13)$$

where $\mu_o = [1-(R_*/R)^2]^{1/2}$. The first member of (13) represents the diffuse component and the second is the scattered stellar radiation field. For extreme cases: $\tau \ll 1$ and $\tau \to 1$, (13) reduces to the known simplified expression $J_\lambda \sim S_\lambda[1-e^{-2\tau_\lambda}] + WF_\lambda^* e^{-2\frac{\tau_\lambda}{\mu_o}}$ (Mihalas 1978), where $W = (1/2)(1-\mu_o)$ is the geometrical dilution factor. Having introduced the opacity ratio ϵ_λ in the source function, the characteristics of the BD will be due to the absorption discontinuity not only through the absorption/emission terms $e^{-\tau_\lambda}$ but also to the discontinuous source function S_λ given by (12).

To test the validity of the approximations made to calculate the angle dependent radiation fluxes, we compare in Fig. 8 the magnitude differences ΔV obtained from (11)(full lines) with those predicted by a Monte Carlo simulation (open dots) (Höflich & Zorec 1989, Höflich 1991) as a function of the aspect angle i. Both calculations refer to a system where the central star has $T_{\rm eff} = 22000\,{\rm K}$ and $R_* = 5R_\odot$, and an ellipsoidal CE with $E = 0.3$ where the density distribution follows the $n = 2$ law. The CE has a constant temperature $T = 0.8T_{\rm eff}$, equatorial extension $R - R_* = 2R_*$, base electron densities (a): $N_{\rm e}^* = 2.5 \times 10^{12}$ and (b): $N_{\rm e}^* = 5.8 \times 10^{12}\,{\rm cm}^{-3}$. We can see, that despite the roughness of our model, it closely reproduces the global variation of ΔV against i predicted by the Monte Carlo method.

3.2.3. Temperature of the CE emitting region

Except for rare examples, models of CE in Be stars assume either a constant temperature $T_{\rm e} \simeq 0.8T_{\rm eff}$ or $T_{\rm e} \simeq 10^4\,{\rm K}$ whatever the photospheric effective temperature. In both cases the choice of $T_{\rm e}$ is independent of the CE density and/or its optical depth. Recently Millar & Marlborough (1998) discussed the temperature structure in Poeckert & Marlborough's (1978a) CE model for γ Cas. Assuming that the diffuse radiation in the CE can be neglected, they obtain that the temperature in the CE is $T_{\rm e} < 0.8T_{\rm eff}$ and fairly constant up to 100 R_*. It ranges from $10^4\,{\rm K}$ in the dense equatorial plane to about $1.5 \times 10^4\,{\rm K}$ in the less dense regions.

This result can be qualitatively understood as follows. In dense layers ($N_{\rm e}^* \gtrsim 10^{13}\,{\rm cm}^{-3}$) where collisional ionization rates of H dominate, the temperature should approach $T_{\rm e} \sim 10^4\,{\rm K}$. In less dense CE regions, where photoionizations and radiative recombinations dominate, the ionization energy is provided by stellar irradiation. As in Be stars ionization of H atoms comes mostly from the Balmer level (Höflich 1988 and Millar, private comm.). Combining the statistical and radiative equilibrium conditions [as done for the Lyman level (Cayrel 1963, Cram 1978)] we obtain: $\int_{\nu_{\rm Ba}}^\infty \sigma_\nu B_\nu(T_{\rm e})/{\rm h}\nu{\rm d}\nu / \int_{\nu_{\rm Ba}}^\infty \sigma_\nu B_\nu(T_{\rm e}){\rm d}\nu \simeq \int_{\nu_{\rm Ba}}^\infty \sigma_\nu \frac{J_\nu}{{\rm h}\nu}{\rm d}\nu / \int_{\nu_{\rm Ba}}^\infty \sigma_\nu J_\nu {\rm d}\nu$, which implies that $T_{\rm e} \simeq T_{\rm Ba}$, the mean temperature of the photospheric Balmer continuum formation regions. Using the Kurucz' (1994) models of stellar atmospheres we get $T_{\rm Ba} = T_{\rm e}(\tau_{\rm Ba} = 1)$. These values can be reproduced with the interpolation formula: $T_{\rm Ba} \simeq 9 \times T_{\rm eff}^{0.73}$. For $T_{\rm eff} = 25000\,{\rm K}$ used for γ Cas, it follows that $T_{\rm e} \simeq 14500\,{\rm K}$, close to Millar & Marlborough's (1998) temperature estimate for layers where the density is $N_{\rm e}^* \lesssim 10^{12}\,{\rm cm}^{-3}$. For SPh-E phases we shall then assume $T_{\rm e} = T_{\rm Ba}$.

In CE where densities are expected to be rather high, we should have $T_{\rm e} \sim 10^4\,{\rm K}$ and even lower. This may be suited for SPh-A phases, as discussed in MZH, where it was shown that the second component of the BD during a SPh-A phase deepens in absorption while $T_{\rm e}$ decreases according to an increase of the CE total optical depth.

3.3. Results of calculations

In Sect. 2.2 it was noted that SPh-A slopes do not show any detectable dependence on aspect-angle and on effective temperature, as we have $\bar{\rm a}_{\rm V} \simeq \bar{\rm a}_\Phi \simeq \bar{\rm a}_{\Phi V} \simeq 0$. So, calculations here below concern SPh-E phases only. On the other hand, only $\rm a_V$ and $\rm a_\Phi$ SPh slopes are worth studying with models because they seem to show the most noticeable $\sin i$ and $T_{\rm eff}$ dependencies.

3.3.1. SPh energy distributions

Before going on to predictions of characteristics of SPh parameters, in the present section we shall answer very briefly goal (c) mentioned in Sect. 3.2. To do so, we show in Fig. 9 the energy distributions obtained by (11) for a same model-Be star, seen in a SPh-E and in a SPh-A phase. This calculation was done for a B2IV-V central star: $T_{\rm eff} = 22000\,{\rm K}$, $R_* = 5.7R_\odot$, log g = 3.9. In both phases $n = 2$. Temperatures for the studied CE zones were adopted as discussed in Sect. 3.2.3: $T = T_{\rm Ba} = 13300\,{\rm K}$ for SPh-E and $T = 10^4\,{\rm K}$ for SPh-A. According to Höflich & Zorec's (1989) results, we used $E = 0.7$ and $i = 45^o$. The remaining free parameters $N_{\rm e}^*$ and $R_{\rm e}/R_*$ were chosen so as to reproduce the mean observed values of $\Delta D < 0$ and $\Delta V < 0$. The CE model parameters hence used and the resulting SPh quantities are resumed in Table 3.

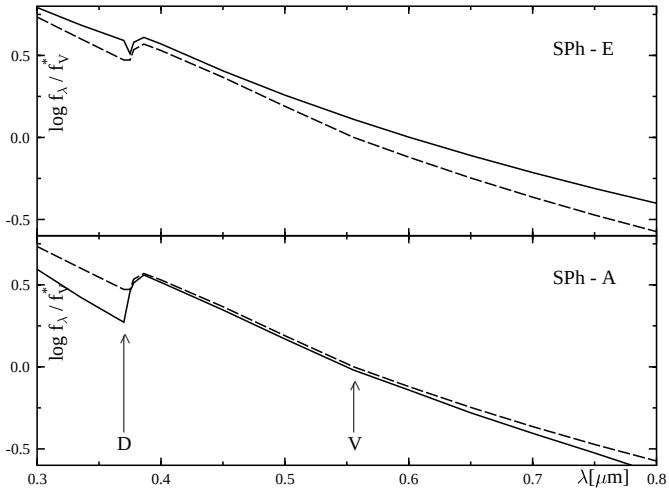

Fig. 9. Model SPh-E ($\Delta V = -0.27$ mag; $\Delta D = -0.09$ dex) and SPh-A ($\Delta V = +0.05$ mag; $\Delta D = +0.20$ dex) energy distributions normalized to the photospheric flux at $\lambda = 0.56\,\mu$m. The dashed line represents the photospheric energy distribution for $T_{\rm eff} = 22000$ K and log g = 3.9

Table 3. Model parameters characterizing the energy distributions shown in Fig. 9.

Phase	$\tau_{\rm e}$	$\tau^{\rm V}$	$\log N_{\rm e}^*$ cm^{-3}	$R_{\rm e}/R_*$	ΔV mag	ΔD dex
SPh-E	0.70	0.09	12.5	3.7	−0.27	−0.09
SPh-A	1.20	0.61	12.8	2.4	+0.05	+0.20

At once we can see that for the SPh-E phase the model reproduces an intrinsic reddening of the Paschen continuum that accompanies $\Delta D < 0$ and $\Delta V < 0$. In the SPh-A phase we note that there is a $\Delta D > 0$ with a very small absorption ΔV and that there is almost no reddening in the Paschen continuum, as shown by observations (Sect. 1.1). For both phases we have $N_{\rm e}^* < 10^{13}$ cm^{-3}, $R_{\rm e}/R_* < 4$ and the CE region producing the SPh-A aspect is more compact (denser and less extended) than that producing the SPh-E phase, as previously discussed in MZH. It follows then that rather small changes in density, extent and temperature of the CE can be sufficient to explain SPh phase variations in a given Be star.

3.3.2. Assumed CE variations

As it is outside the scope of this paper to calculate in detail SPh variations produced by changes of the CE structure due to dynamic phenomena driven by successive more or less continuous or discrete mass loss events, we shall only sketch them assuming three extreme cases: (a) Surrounding the star there is an elliptical expanding shell (literal meaning) whose mass and ellipticity are maintained. The mass of the shell is parametrized through an initial scattering optical depth $\tau_{\rm e}^p$ measured in the polar direction; (b) Expanding shell as in (a), but the shell evolves preserving the vertical semi-axis h, so that its equivalent ellipticity is variable as the shell expands: $E = h/R_{\rm e}$ (for simplicity we used $h = R_*$); (c) The CE has constant ellipticity ($E =$ const) and equatorial extent ($R_{\rm e} =$ const), but its density increases with time.

Table 4. Parameters characterizing the case (a) of SPh variations with $E = 0.3$, $i^o = 30$ and initial $\tau_{\rm e}^p = 1$

$R_{\rm e}/R_*$	$\log N_{\rm e}^*$	$\tau_{\rm V}$	ΔV mag	ΔD dex
1.1	12.53	1.54	-0.013	-0.011
2.0	12.20	0.68	-0.494	-0.194
3.0	11.85	0.42	-0.345	-0.243
4.0	11.60	0.30	-0.197	-0.202
7.0	11.30	0.17	-0.055	-0.097

For all three cases we assumed that the particle density distribution is preserved with $n = 2$ even if the shape of the CE will change. The central star was characterized by $T_{\rm eff} =$ 22000 K and $R_*/R_\odot = 5.7$. In all calculations we used $\tau_{\rm e}^p \lesssim 1$; $1.0 \leq R_{\rm e} \leq 10$ and we always used the same parametrization steps: $\Delta R_{\rm e}/R_* = 0.1$; $\Delta N_{\rm e}^*/10^{12} = 0.05$ to better appreciate possible differences in rates of SPh variations. Each time the parametrization implied a total optical depth $\tau/\Lambda(E,i) \gtrsim 3$ calculations were stopped.

As an exemple for properties of models discussed in the next section for explaining (a) variations, the following model parameters are listed in Table 4 for five steps of the development of a CE having $E = 0.3$: R/R_* = CE total equatorial extent; $N_{\rm e}^*$ = base electron density; $\tau_{\rm V} = \tau_{\rm e} + \tau^{\rm V}$ = total radial opacity for $\lambda = 0.56\,\mu$m in the direction i; ΔV and ΔD that reproduce the SPh variations for case (a) with $i = 30^o$ and a layer with initial $\tau_{\rm e}^p = 1$, which corresponds to $N_{\rm e}^* = 3.8 \times 10^{12}$ cm^{-3} and an ejected mass $\Delta M \simeq 6 \times 10^{-11} M_\odot$ roughly.

3.3.3. Main characteristics of results obtained

Characteristics of the aspect angle dependency of the ΔV variations against ΔD are depicted in Fig. 10. Case (a) is illustrated for $\tau_{\rm e}^p = 1$, three constant ellipticities: $E =$ 0.1, 0.3, 0.7 and for aspect angles: i^o = 0, 30, 50, 60, 70, 80 and 90. Case (b) is illustrated for initial densities represented by $\tau_{\rm e}^p =$ 0.5, 0.7, 1 and for the same aspect angles as in case (a). Case (c) is illustrated for the same ellipticities as in (a) and for two CE extents: $R_{\rm e} = 2.5$ (points), 6 (crosses). In case (c) densities range from $N_{\rm e}^* = 10^9$ (where $\Delta V \simeq \Delta D \simeq 0$) to 5×10^{12} cm^{-3}. For $R_{\rm e} = 2.5$ results are shown for $i^o = 0$, 30, 50, and 90, while for $R_{\rm e} = 6$ they are also given for $i^o = 60$, 70, 80 and 90. Other results for different effective temperatures and $\tau_{\rm e}^p$ are shown numerically in Table 5. The SPh slopes were obtained using the least squares method in the BD interval $-0.2 \leq D \leq 0.0$. In this variation interval of D, which corresponds to that most frequently observed, a number of combinations of model parameters lead to SPh curves that strongly deviate from linear behaviour or simply there is no SPh $(\Delta V, \Delta D)$ relation, which justifies some missing SPh curves in Fig. 10 or missing slopes in Table 5. Other missing curves are discussed in Sect. 3.3.4.

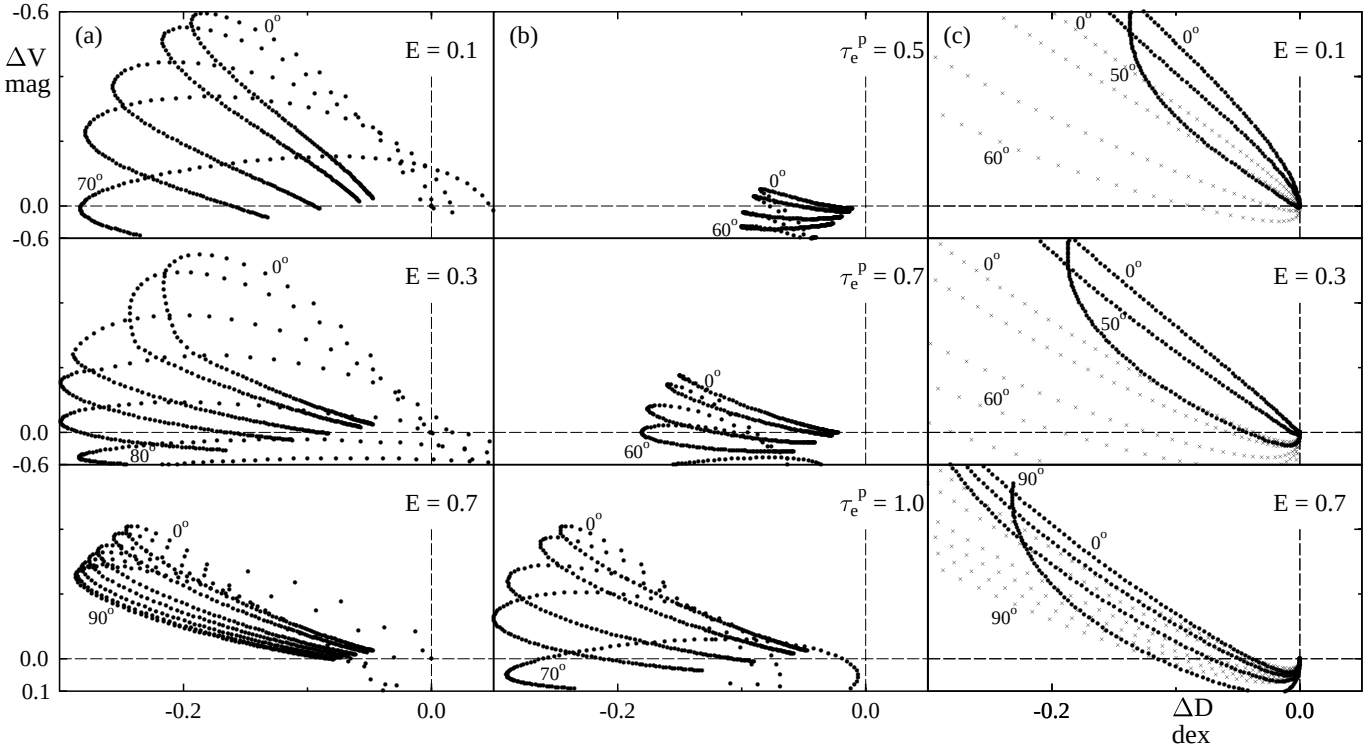

Fig. 10a–c. ΔV variations against ΔD for several CE configurations. Case **a**: expanding envelope with E = constant. Case **b**: expanding envelope with E = variable but $h = R_*$. Case **c**: variable density in a CE with constant volume. In **c** points are for $R_e = 2.5$ and crosses for $R_e = 6$

The obtained results can be summed up as follows:

1 – Observed amplitudes (typically less than or equal to 0.5 mag) of ΔV variations can be accounted for with events of type (a) to (c) using densities $N_e^* \lesssim 10^{13}\,\mathrm{cm}^{-3}$ and equivalent CE extents $R_e \lesssim 3$ [roughly the turnover point of the $(\Delta V, \Delta D)$ loops in (a) and (b)]. Emissions are as a mean the strongest the more flattened the CE, but only for $i \lesssim 60^o$. In strongly flattened CE emission in V is lost for $i \gtrsim 70^o$ and when $\tau_e^p \lesssim 0.7$. However, emission in V produced in CE with more moderate flattenings ($E \sim 0.7$) is seen from whatever aspect angle, though $|\Delta V|$ can be somewhat smaller. In case (b), which more closely corresponds to a disc-like configuration, the emission in the V magnitude is lost at inclinations $i^o \gtrsim 77(\tau_e^p)^{1.2}$ and/or when $\tau_e^p \lesssim 0.7$, quite similarly as in Poeckert & Marlborough's (1978a,b) models [Sect. 3.1(f)].

2 – For a given choice of E and i, amplitudes of ΔV and ΔD variations are a function of τ_e^p. To produce by processes (a) or (b) BD discrepancies $\Delta D \sim -0.3$ dex, which are similar to the mean observed ones (Zorec & Briot 1991, Ballereau et al. 1995), the amount of gathered mass in the CE is characterized by $0.7 \lesssim \tau_e^p \lesssim 1$. However, if the same amount of emission in V is expected to be produced by process (b), we would not only need $i \lesssim 60^o$ but also $\tau_e^p \gtrsim 1$ which can easily conflict with the density limitations discussed in Sect. 3.1(b).

3 – Most of the calculated a_V slopes in SPh-E phases are positive. However, negative ones, although rarely observed, are expected for very flattened CE seen nearly equator-on (ex. $E = 0.1$, $i = 70^o$).

4 – Events of type (a) and (b) produce **"double valued"** a_V and a_Φ slopes so that two phases are distinguished, which are discussed in Sect. 3.3.4.

5 – Process (c) produces a single valued a_V slope, which is a function of E, i and R_e. At given values of E and i the rate $-(\partial V/\partial\tau)$ strongly depends on R_e. When $E \lesssim 0.5$ at inclinations from $i \gtrsim 50^o$ to 60^o, respectively for $R_e = 2.5$ to 6, in (c) it is $\Delta V > 0$ even though $\Delta D < 0$ as long as opacity $\tau/\Lambda(E,i) \leq 1.5$. For compact CE ($R_e = 2.5$) when $\tau/\Lambda(E,i) > 1.5$, the SPh evolution is characterized by $\Delta D \sim$ constant and a strong emission rise in the magnitude V. In more extended CE ($R_e = 6$) there is a single monotonic slope in the commonly observed variation interval of ΔD, whatever the inclination. The same ΔD and ΔV differences are obtained in the more extended CE using lower values of N_e^* than in the compact ones.

6 – Processes (a) and (b) produce $a_\Phi < 0$ as observed in most Be stars. Process (c) leads to a reddening effect of the visible energy distribution, but the reddening decreases as emission increases so that $a_\Phi > 0$. This effect was also observed, though rarely.

Finally we note that for given aspect-angle and effective temperature, but depending on the value of τ_e^p as well as on the degree to which one of the above processes is dominant, a wide variety of SPh slopes can be obtained. This accounts for significant dispersion of SPh slopes among stars with similar fundamental parameters, as seen in Figs. 2 to 5. On the other hand, an effective temperature dependency of SPh slopes can be derived from inspection of Table 5 which is in the direction

Table 5. SPh slopes calculated for cases (a) and (c). Values are presented by couples $a_V|a_\Phi$ (mag dex^{-1}|μm dex^{-1})

	Case (a)			$\tau_e^p = 0.5$				$\tau_e^p = 1.0$			
i^o	E	sol.	$T_{\rm eff}$ = 12500	16500	22000	30000	12500	16500	22000	30000
0	0.1	u	1.75|-1.15	1.56|-0.98	2.69|-1.42	..|..	2.91|-1.67	3.02|-1.44	2.88|-1.55	5.62|-2.57
		l	..|..	1.48|-0.81	3.97|-1.44	..|..	..|..	..|..	3.27|-1.49	2.51|-3.01
	0.3	u	1.62|-1.16	1.36|-0.98	2.13|-1.43	..|..	2.84|-1.70	2.79|-1.45	2.56|-1.57	4.60|-2.58
		l	..|..	0.56|-0.80	2.96|-1.44	..|..	..|..	..|..	1.44|-1.48	2.59|-3.44
	0.7	u	0.73|-1.29	0.36|-1.06	1.23|-1.47	..|..	..|..	1.59|-1.53	1.34|-1.65	1.10|-2.56
		l	..|..	0.56|-0.80	0.82|-1.45	..|..	..|..	..|..	1.44|-1.48	0.54|0.04
	1.0	u	3.21|-1.48	2.57|-1.16	4.08|-1.46	..|..	..|..	7.49|-1.67	6.29|-1.64	9.79|-2.35
		l	..|..	0.56|-0.80	0.87|-1.45	..|..	..|..	..|..	1.44|-1.48	0.47|0.15
30	0.1	u	1.96|-1.41	1.38|-0.94	2.48|-1.27	..|..	3.19|-1.96	2.82|-1.58	2.57|-1.46	5.18|-2.25
		l	..|..	1.18|-0.71	3.13|-1.31	..|..	..|..	..|..	2.67|-1.34	2.64|-2.88
	0.3	u	1.73|-1.40	1.25|-0.97	2.11|-1.31	..|..	2.88|-1.97	2.71|-1.62	2.43|-1.52	3.98|-2.29
		l	..|..	0.41|-0.72	1.99|-1.33	..|..	..|..	..|..	1.16|-1.35	2.84|-3.15
	0.7	u	1.00|-1.45	0.56|-1.08	0.20|-1.33	..|..	..|..	1.68|-1.67	1.62|-1.67	2.01|-2.37
		l	..|..	0.48|-0.76	0.62|-1.40	..|..	..|..	..|..	1.29|-1.41	0.53|0.05
60	0.1	u	0.81|-0.55	0.42|-0.35	0.73|-0.46	..|..	2.35|-2.35	1.56|-1.58	0.99|-0.98	1.32|-1.07
		l	..|..	0.45|-0.38	0.73|-0.74	..|..	..|..	..|..	1.25|-0.87	2.97|-2.66
	0.3	u	0.14|-0.88	0.24|-0.40	0.67|-0.81	..|..	1.95|-1.38	0.93|-1.32	0.73|-1.02	1.13|-1.33
		l	..|..	0.05|-0.44	..|..	..|..	..|..	..|..	0.47|-0.97	0.55|-2.34
	0.7	u	1.07|-0.78	1.05|-0.66	0.28|-1.02	..|..	5.36|-2.08	3.40|-1.57	2.35|-1.36	3.80|-1.73
		l	..|..	0.30|-0.64	..|-1.27	..|..	..|..	..|..	0.95|-1.25	0.55|0.07
90	0.1		..|..	..|..	..|..	..|..	..|..	..|..	..|..	..|..
	0.3		..|..	..|..	..|..	..|..	..|..	..|..	..|..	..|..
	0.7	u	0.59|-0.45	0.75|-0.46	..|..	..|..	..|-1.93	2.40|-1.32	1.98|-1.07	3.04|-1.27
		l	..|..	..|..	..|..	..|..	..|..	..|..	0.76|-1.14	0.55|..
	Case (c)			$R_e = 2.5$				$R_e = 6.0$		
i^o	E	sol.	$T_{\rm eff}$ = 12500	16500	22000	30000	12500	16500	22000	30000
0	0.1		0.81|0.31	1.90|0.73	3.79|1.44	6.12|2.30	0.53|0.19	1.32|0.48	2.87|1.05	5.39|2.00
	0.3		0.54|0.19	1.45|0.53	3.24|1.21	5.69|2.12	0.30|0.09	0.90|0.30	2.30|0.81	4.95|1.81
	0.7		0.35|0.11	0.96|0.32	2.60|0.94	5.21|1.91	0.30|0.09	0.90|0.30	2.30|0.81	4.95|1.81
	1.0		0.35|0.11	0.96|0.32	2.60|0.94	5.21|1.91	0.30|0.09	0.90|0.30	2.30|0.81	4.95|1.81
30	0.1		0.69|0.26	1.69|0.64	3.59|1.35	5.80|2.15	0.39|0.14	1.06|0.38	2.43|0.88	4.71|1.74
	0.3		0.43|0.15	1.22|0.44	2.93|1.08	5.32|1.95	0.20|0.05	0.71|0.23	1.94|0.68	4.36|1.56
	0.7		0.31|0.09	0.85|0.28	2.41|0.86	4.98|1.81	0.25|0.07	0.80|0.26	2.10|0.74	4.63|1.68
60	0.1		0.57|0.20	1.42|0.52	6.06|2.27	9.36|5.57	0.07|0.02	0.35|0.11	1.26|0.38	2.89|1.03
	0.3		0.28|0.11	0.84|0.28	5.19|1.53	7.56|2.90	-0.02|-0.02	0.20|0.06	1.00|0.32	2.80|0.91
	0.7		0.24|0.06	0.70|0.20	2.07|0.72	4.88|1.73	0.12|0.03	0.57|0.18	1.66|0.57	3.90|1.37
90	0.1		0.49|0.17	1.26|0.45	..|..	..|..	-0.08|-0.04	0.07|0.01	0.79|0.20	2.57|0.76
	0.3		0.19|0.09	0.64|0.20	..|..	..|..	-0.13|-0.06	-0.01|-0/01	0.57|0.16	2.08|0.54
	0.7		0.20|0.04	0.71|0.22	2.11|0.72	5.40|1.89	0.05|0.00	0.43|0.12	1.40|0.47	3.46|1.19

Note: Letters "u" and "l" in column Sol. (solutions) in case (a) are respectively for "upper" and "lower" braches of $(\Delta V, \Delta D)$ loops.

depicted by the statistical results of Figs. 2 to 5. However, actual temperature dependency may still be different, depending on the model used and on the combination of CE parameters.

3.3.4. Discussion

Though probably cases (a), (b) and (c) do not represent individually an actual dynamic behaviour/evolution of CE, they can be thought of as extreme CE variation frames to explore the first order effects on SPh changes produced by CE as different as discs and spheroids. In particular, they give as clue to understanding the double valued SPh slopes, which is intrinsically important, because it leads us to a possible mechanism of CE formation in Be stars. The double valued SPh slopes can be understood in terms of well known optical depth variations of expanding shells (Ambartsumian 1966, Sobolev 1990). Two main phases are distinguished. In the first phase, the opacity of the shell (literal meaning) is rather high and the photometric evolution of the system is determined by the increase of R_e. It corresponds to the upper part of $(\Delta V, \Delta D)$ loops in Fig. 10. Assuming the mass

of the expanding shell is preserved, it can be easily shown that opacity is a decreasing function of $R_{\rm e}$, if $n = 2$ in the particle density distribution function. The emission in V and D reduces accordingly. This characterizes the second phase, the lower part of the $(\Delta V, \Delta D)$ loops in Fig. 10. The gradient $-(\partial V/\partial\tau)$ is stronger in the first phase (rapid variation) than in the second phase (slow variation).

If behaviours (a) and (b) are to be driven by an isolated huge mass ejection, an initial value $\tau_{\rm e}^p \sim 1$ implies that a shell of mass $\Delta M/M_\odot \sim (10^{-10} - 10^{-9}) \times E$ would be ejected. The same effect can also be obtained if there is a low-density circumstellar environment where a snowplough like drag of mass is set up by less massive ejecta. The mentioned 'second phase' will then exist whenever the rate of accumulating mass in the shell, due to the snowplough effect, does not prevent an opacity decrease produced by the expansion of the outermost layers. Phases of isolated massive ejections, a possible explanation of light outbursts described by Hubert et al. (1997) and Hubert & Floquet (1998), can then be followed by more or less variable continuous mass loss that fills up the environment emptied by the dragged out matter. The latter corresponds in a way to the phenomenon described by case (c). In such an interpretation, the building up of CE in Be stars will then be due to sequences of phases with massive 'parcel' ejections, followed by continuous mass loss phenomena. This generalizes the mechanism of CE formation by sequences of variable mass loss events proposed by Zorec (1981). The massive isolated ejections might finally also initiate non-radial global oscillations in CE, which are thought today to produce the V/R line variations (Okazaki 1991, 1996, Hanuschik et al. 1995). We note however, that the density perturbations needed to explain the V/R variations are so tiny that they cannot be responsible for any noticeable SPh changes like those studied in the present paper.

We note that there is still an additional physical reason which explains some missing $(\Delta V, \Delta D)$ relations in Fig. 10 and missing slopes in Table 5. They correspond to highly flattened CE configurations, where in some wavelength regions we obtain $\tau_\lambda \to \tau_\lambda^p/E \gtrsim 3$ as $i \to \pi/2$. In such limits we frequently have $\Delta V \gtrsim 0$, while $\tau_\lambda \gtrsim 2$ in the near-UV carries $\Delta D < 0$ implying a strong continuous emission. However, for those wavelengths where $\tau_\lambda \gtrsim 3$ the CE behaves as a pseudo-photosphere and an approximation like (11) is probably no longer suitable. As in classic Be stars, whatever the SPh phase, there is always a distinguishable underlying photospheric energy distribution in the Paschen continuum near the BD [but with rare exceptions such as γ Cas in 1932–42 (Chalonge & Safir (1936)], the fact that for $i \to \pi/2$ in strongly flattened CE we obtain $\tau_\lambda \gtrsim 3$, a base density $N_{\rm e}^* = 5 \times 10^{12}$ cm^{-3} leading to $\tau_{\rm e}^p = 1.0$ in cases (a) and (b) may be considered as too high, though density limits established in Sect. 3.1(b) are not violated.

It is worth noting that due to the number of CE parameter combinations which lead to similar SPh quantities and the variety of CE geometrical configurations implied by double valued SPh behaviours, it can hardly be maintained that the observed SPh phenomena in a given Be star can be explained in the framework of a unique and constant geometry of CE.

We conclude that the main characteristics of the observed SPh behaviours were schematically described using simple models with parameters: $R_{\rm e}$, $T_{\rm e}$ and $N_{\rm e}^*$ whose values are not beyond the limits imposed by observations. These models can account for: amplitudes of ΔV, ΔD and $\Delta\Phi_{\rm rb}$ variations; single and bivalued SPh slopes; signs and absolute values of $a_{\rm V}$ and a_Φ SPh slopes; mean aspect-angle and temperature dependencies of SPh slopes that compare with those shown in Figs. 2 to 5. However, as the combinations of model parameters and physical frames producing a given SPh variation from star to star and even in the same star at different epochs are numerous, stars should be analyzed individually to determine the type of phenomenon that most likely produces an observed SPh variation. Only then should estimates of CE mean densities, temperatures, extents and ellipticities be used to produce averages of SPh slopes that can be compared with the statistical results shown in Figs. 2 to 5. We finally note that the SPh slopes we calculated in this work were obtained for electron distributions with $n = 2$. However, as the discussion of characteristics of SPh variations dependent on the value of n is outside the scope of the present paper, it will be given elsewhere.

Let us finally note that the light outbursts found by Hubert & Floquet (1998), which the most likely correspond to type (a) or (b) variations, have characteristic time scales of the order of 1 year. To confirm the counter-clockwise loop-like SPh behaviours described in this paper, regular multicolour photometric and/or SPh observations should have been carried out during the whole time elapsed by these phenomena. On the other hand, light outbursts of short time scales (days), which can also imply discontinuous mass ejection events, were reported in the literature (Štefl et al. 1994). However, successive discontinuous mass ejection events, will produce a series of colliding layers with backward anf forward directed shocks, that cannot be treated with the simple scenarios presented here. Though we have foreseen the possibility of loop-like SPh behaviours, those reported in MZH may actually correspond to physical frames that widely spill the simple ones studied in this paper.

4. Conclusions

In this paper we have reviewed long-term visual spectrophotometric (SPh) variations of Be stars using an exhaustive set of data presented in a previous paper (MZH). We studied the SPh variations as a function of fundamental stellar parameters. The data used allowed us to confirm and generalize previous results obtained by us and other authors. We noted in addition that there are $V \sin i$ and $T_{\rm eff}$ dependencies of SPh variations. We paid much attention to the interpretation of bivalued $(\Delta V, \Delta D)$ SPh relations that were put forward in our preceding paper MZH. The observed SPh behaviours of Be stars were described as a function of three CE variation scenarios: (a) CE expansion by preserving ellipticity; (b) CE expansion by varying the ellipticity so that a disc-like structure is produced; (c) filling up a constant circumstellar volume with given extent and flattening. CE base densities and extents of regions producing the SPh variations were adopted according to a previous critical discussion

of model consistencies with observational facts. From this discussion it follows that electron density in CE of Be stars should never exceed $N_{\rm e} \sim 10^{13}\,{\rm cm}^{-3}$ and that the radii of regions producing the SPh do not exceed some R_*. It was also shown that SPh observations do not always support strongly flattened CE. Models show that in such flattened CE it is not possible to produce the amount of emission currently observed in the V magnitude without violating the CE density limitations imposed by the characteristics of the second component of the Balmer discontinuity. The double valued $(\Delta V, \Delta D)$ relations are due to the opacity evolution of CE in processes (a) and (b). These scenarios are consistent with a building up mechanism of CE in Be stars due to isolated massive ejections, followed by continuous mass loss phenomena. The models of axi-symmetrical CE used in this paper explain the global aspect angle and temperature dependencies of SPh slopes, though detailed studies of individual stars are needed to identify the CE variation scenarios which are most likely to account for the observed facts and to lead to the most reliable set of CE physical parameters.

Acknowledgements. This research has made use of several databases and abstract services: Centre de Données Stellaires de Strasbourg (CDS), The General Catalogue of Photometric Data (GCPD, University of Lausanne), Astronomical Data Analysis Center (ADAC, NAO Japan) and NASA's Astrophysics Data System Abstract Service (ADS). Criticisms of Pr. J. Dachs on preceding versions of the paper are acknowledged as they encouraged substantial improvements. We are grateful to Dr. E. Simonneau for advice on radiation transfer simplifications used in the paper and to Drs. J. De Freitas Pachéco, L. Houziaux and Ph. Stee for fruitful discussions. Many thanks are due to A. Garcia for preparing the figures.

Appendix A

1 – For elliptical structures where $R_{\rm p} = E \times R_{\rm e} < 1$ the most frequent situations encountered in our calculations can be classified as follows:

(a) $i < i_1$. The angle i_1 is shown in Fig. 7 and is given by $\tan i_1 = y_*/x_*$, where (x_*, y_*), the coordinates in the (x, y) plane of the CE-star interception are:

$$y_* = \Big[\frac{R_{\rm p}^2 - E^2}{1 - E^2}\Big]^{1/2}; \quad x_* = \Big[\frac{1 - R_{\rm p}^2}{1 - E^2}\Big]^{1/2} \tag{14}$$

The uncovered fraction of stellar area projected in the plane perpendicular to the line of sight: $s_{\rm u}(R_{\rm e}, E, i)$, the area of fraccion covered by the CE: $s_{\rm c}(R_{\rm e}, E, i)$ and that of the CE not intercepted by the star: $s_{\rm e}(R_{\rm e}, E, i)$, are given by:

$$s_{\rm u} = x_*^2 \cos i; \;\; s_{\rm c} = 1 - s_{\rm u}; \;\; s_{\rm e} = s_{\rm env} - 1 \tag{15}$$

where $s_{\rm env} = R_{\rm e}^2 \Lambda(E, i)$ is the whole area (in units of the projected stellar area πR_*^2) of the ellipsoidal CE projected on the plane perpendicular to the line of sight and $\Lambda(E, i) = [1 - (1 - E^2)\sin^2 i]^{1/2}$.

(b) $i_1 < i < i_o$. To shorten the writing of mathematical expressions, in what follows we use the following notation which arises from transformation of the representation of the ellipsoidal CE in the (x, y, z) system to another system directed towards the observer:

$$\begin{aligned} l(v, x) &= (v^2 - x^2)^{1/2} \\ l_+(x) &= y_* \sin i + (x_*^2 - x^2)^{1/2} \cos i \\ l_-(x) &= y_* \sin i - (x_*^2 - x^2)^{1/2} \cos i \\ s_o(z) &= \frac{1}{\pi}[\arcsin z + \frac{1}{2}\sin[2 \arcsin z] \end{aligned}$$

The angle i_o between the y-axis and the lower tangent to the CE where the envelope intercepts the star (see Fig. 7) is given by $\tan i_o = E^{-2} \tan i_1$. For the present inclination-angle interval the fractional projected areas are:

$$\begin{aligned} s_{\rm u} &= \frac{2}{\pi}\Big\{\int_0^{x_{\rm p}} l(1, x){\rm d}x + \int_{x_{\rm p}}^{x_*} l_+(x){\rm d}x - \int_0^{x_*} l_-(x){\rm d}x\Big\} \\ &= x_*^2 \cos i[1 - s_o(x_{\rm p}/x_*)] - \frac{2}{\pi} y_* x_* \sin i + s_o(x_{\rm p}) \end{aligned} \tag{16}$$

where x_p, the x coordinate of the intersection of the stellar limb with the CE:

$$x_{\rm p} = (1 - \frac{y_*^2}{\sin^2 i})^{1/2} \tag{17}$$

For the remaining fractional areas we have:

$$s_{\rm c} = 1 - s_{\rm u}; \quad s_{\rm e} = s_{\rm env} - s_{\rm l} \tag{18}$$

where:

$$\begin{aligned} s_{\rm l} &= 1 - \frac{2}{\pi}\Big\{\int_0^{x_{\rm e}} [l(1, x) - \Lambda(E, i) l(R_{\rm e}, x)]{\rm d}x \\ &= 1 - [2 s_o(x_{\rm e}) + R_{\rm e}^2 \Lambda(E, i) s_o(x_{\rm e}/R_{\rm e})] \end{aligned} \tag{19}$$

for $R_{\rm e} < \Lambda(E, i)^{-1}$ and $s_l = 1$ for $R_{\rm e} \geq \Lambda(E, i)^{-1}$. In the above expressions we have:

$$x_{\rm e} = \Big[\frac{1 - R_{\rm e}^2 \Lambda^2(E, i)}{1 - \Lambda^2(E, i)}\Big]^{1/2} \tag{20}$$

(c) $i > i_o$.

$$\begin{aligned} s_{\rm u} &= \frac{2}{\pi}\Big\{\int_0^{x_{\rm p}} l(1, x){\rm d}x + \int_{x_{\rm p}}^{x_*} l_+(x){\rm d}x - \int_0^{x_*} l_-(x){\rm d}x \\ &\quad + \int_0^{x_*} [l(1, x) - l_+(x)]{\rm d}x\Big\} \\ &= x_*^2 \cos i[\frac{1}{2} - s_o(x_{\rm p}/x_*)] - \frac{2}{\pi} y_*(x_* + x_{\rm p}) \sin i \\ &\quad + s_o(x_{\rm p}) - s_o(x_{\rm p}/x_*) \end{aligned} \tag{21}$$

As in preceding cases, we have now:

$$s_{\rm c} = 1 - s_{\rm u}; \quad s_{\rm e} = s_{\rm env} - s_{\rm l} \tag{22}$$

where:

$$\begin{aligned} s_{\rm l} &= 1 - \frac{2}{\pi}\int_0^{x_*} [l(1, x) - l_+(x)]{\rm d}x \\ &= 1 - [\frac{1}{2} x_*^2 \cos i + \frac{2}{\pi} y_* x_* \sin i + s_o(x_*)] \end{aligned} \tag{23}$$

2 – In all cases where $R_{\rm e} \geq R_*$, it is: $s_{\rm u} = 0$, $s_{\rm c} = 1$ and $s_{\rm e} = s_{\rm env} - 1$ for all values of i.

References

Ambartsumian V.A., 1966, Theoretical Astrophysics. Spanish transl. EUDEBA, p. 514
Araújo F.X., Freitas Pacheco J.A., 1989, MNRAS 241, 543
Ballereau D., Chauville J., Zorec J., 1995, A&AS 111, 423
Barbier D., Chalonge D., 1939, ApJ 90, 627
Barbier D., Chalonge D., 1941, Ann. Astrophys. 4, 30
Beeckmans F., 1976, A&A 52, 465
Bjorkman J.E., Cassinelli J.P., 1993, ApJ 409, 429
Bodenheimer P., 1971, ApJ 167, 153
Cayrel R., 1963, CRASP 257, 3309
Chalonge D., Safir H., 1936, CRASP 203, 1329
Chalonge D., Divan L., 1952, Ann. Astrophys. 15, 201
Chalonge D., Divan L., 1973, A&A 23, 69
Cram L.E., 1978, A&A 138, 301
Dachs J., 1982, In: Jaschek M., Groth H.G. (eds.) IAU Symp. No. 98, Be Stars. Reidel, p. 19
Dachs J., Engels D., Kiehling R., 1988, A&A 194, 189
Dachs J., Hanuschik R., 1984, A&A 138, 140
Dachs J., Poetzel R., Kaiser D., 1989, A&AS 78, 487
Divan L., 1979, In: McCarthy M.F., Philip A.G.D., Coyne G.V. (eds.), IAU Coll. No. 47, Spectral Classification of the Future. Vatican Obs., p. 247
Divan L., Zorec J., 1982, In: Perrymann M.A.C., Guyenne T.D. (eds.) The Scientific Aspects of the Hipparcos Space Astrometry Mission. ESA-SP 177, p. 101
Divan L., Zorec J., Briot D., 1982, In: Jaschek M., Groth H.G. (eds.), IAU Symp. No 98, Be Stars. Reidel Publ. Co., p. 53
Gulliver A.F., 1977, ApJS 35, 441
Hanuschik R.W., Hummel W., Sutorius E., et al., 1996, A&AS 116, 309
Hanuschik R.W., Hummel W., Dietle O., et al., 1995, A&A 300, 163
Hirata R., 1982, In: Jaschek M., Groth H.G. (eds.) IAU Symp. No. 98, Be Stars. Reidel, p. 41
Hirata R., Hubert-Delplace A.M., 1981, In: G.E.V.O.N., Sterken C. (eds.), Workshop on pulsating B stars. Obs. de Nice, p. 217
Hirata R., Kogure T., 1976, PASJ 28, 509
Hirata R., Kogure T., 1984, Bull. Astr. Soc. India 12, 109
Höflich P., 1988, A&A 191, 348
Höflich P., 1991, A&A 246, 481
Höflich P., Sharp Ch.M., Zorec J., 1989, in: Norman E.B. (ed.) Particle Astrophysics Workshop, Berkeley, World Science, p. 186
Höflich P., Zorec J., 1989, In: Delache P., Laloë S., Magnan C., et al. (eds.) Modeling the Stellar Environment, How and Why? Fourth IAP Meeting, p. 257
Hubert-Delplace A.M., Hubert H., 1979, An Atlas of Be Stars. Paris-Meudon Observatory
Hubert-Delplace A.M., Hubert H., 1981, A&AS 44, 109
Hubert A.M., Floquet M., 1998, A&A 335, 565
Hubert A.M., Floquet M., Gómez A.E., et al., 1997, Proceedings of the ESA Symp. Hipparcos-Venice 97, ESA SP-402, p. 315
Hummel W., 1998, A&A 330, 243
Hummel W., Dachs J., 1992, A&A 262, L17
Kogure T., Hirata R., 1982, Bull. Astr. Soc. India 10, 281
Kurucz R.L., 1994, Model Atmospheres. SAO CD-ROM N*o* 19
Lucy L.B., 1974, AJ 79, 745
Mennickent R.E., Vogt N., Sterken C., 1994, A&AS 108, 237
Mihalas D., 1978, Stellar Atmospheres. Freeman and Co.
Millar C.E., Marlborough J.M., 1998, ApJ 494, 715
Moujtahid A., 1998, Thèse de Doctorat, Université Paris VI
Moujtahid A., Zorec J., Hubert A.M., et al., 1998, A&AS 129, 289 (MZH, Paper I)
Okazaki A.T, 1991, PASJ 43, 75
Okazaki A.T, 1996, PASJ 48, 305
Osterbrock D.E., 1989, Astrophysics of Gaseous Nebulae and Active Galactic Nuclei. University Science Books
Owocki S.P., Cranmer S.R., Blondin J.M., 1994, ApJ 424, 887
Owocki S.P., Cranmer S.R., Gayley K.G., 1996, ApJ 472, L115
Poeckert P., Marlborough J.M., 1978a, ApJ 220, 940
Poeckert P., Marlborough J.M., 1978b, ApJS 38, 229
Porter J.M., 1996, MNRAS 280, L31
Quirrenbach A., Bjorkman K.S., Bjorkman J.E., et al., 1997, ApJ 479, 477
Quirrenbach A., Buscher D.F., Mozurkewich D., et al., 1994, A&A 283, L13
Quirrenbach A., Hummel C.A, Buscher D.F., et al., 1993, ApJ 416, L25
Sackmann I.J., 1970, A&A 8, 76
Slettebak A., 1982, ApJS 50, 55
Slettebak A., Collins II G.W., Truax R., 1992, ApJS 81, 335
Smart W.M., 1958, Combination of Observations. Cambridge Univ. Press
Sobolev V., 1990, Cours d'astrophysique théorique, MIR, p. 416
Stee Ph., Araújo F.X., 1994, A&A 292, 221
Stee Ph., Araújo F.X., Vakili F., et al., 1995, A&A 300, 219
Stee Ph., Vakili F., Bonneau D., et al., 1998, A&A 332, 268
Štefl S., 1998, In: Variable and Non-spherical Stellar Winds in Luminous Hot Stars. IAU Coll. N^o. 169 (in press)
Štefl S., Harmanec P., Baade D., 1994, In: Balona L.A., Henrichs H.F., Le Contel J.M. (eds.), Pulsation, Rotation and Mass Loss in Early-Type Stars. IAU Symp. No. 162, Kluwer Acad. Publ., p. 455
Underhill A., Doazan V., 1982, B Stars With and Without Emission Lines. NASA-CNRS, NASA-SP 456
van Kerkwijk M.H., Waters L.B.F.M., Marlborough J.M., 1995, A&A 300, 259
Vidal C.R., 1966, J.Q.S.R.T. 6, 575
Waters L.B.F.M., 1986, A&A 162, 121
Waters L.B.F.M., Marlborough J.M., 1994, In: Balona L.A., Henrichs H.F., Le Contel J.M. (eds.) Pulsation, Rotation and Mass Loss in Early-Type Stars. IAU Symp. No. 162, Kluwer Acad. Publ., p. 399
Wood K., Bjorkman K.S., Bjorkman J.E., 1997, ApJ 477, 926
Yang S., Walker G.A.H., Hill G.M., et al., 1990, ApJS 74, 595
Zorec J., 1981, In: Chiosi C., Stalio R. (eds.) Effects of Mass Loss on Stellar Evolution, IAU Coll. N^o. 59, p. 539
Zorec J., 1986, Thèse d'Etat, Université Paris VII
Zorec J., Briot D., 1991, A&A 245, 150
Zorec J., Briot D., 1997, A&A 318, 443
Zorec J., Frémat Y., Hubert A.M., 1999, In: Smith M., Henrichs H., Fabregat J. (eds.) The Be Phenomenon in Early-Type Stars. IAU Coll. No. 175
Zorec J., Mochkovitch R., Divan L., 1988, CRASP 506, 1265